CHARLES UNIVERSITY

Faculty of Pharmacy in Hradec Králové

Department of Pharmacology and Toxicology

UNIVERSITY OF LJUBLJANA

Faculty of Pharmacy

The Chair of Clinical Biochemistry

LOCALISATION OF FUBP3 PROTEIN IN HUMAN CERVICAL CANCER CELL LINE

Diploma thesis

Supervisor: Eduard Jirkovský, PharmD, PhD; Assist. Prof. Nika Lovšin, M. Chem., PhD

Ljubljana & Hradec Králové 2020 Josef Kunrt

Hereby I declare, this thesis is my original work. All literature and other sources that I used while processing are listed in the bibliography and properly cited. To my knowledge, this thesis has not been submitted for obtaining the same or any other degree.

Hradec Králové, 11. 5. 2020 Josef Kunrt

Acknowledgements

My great acknowledgement goes to Eduard Jirkovský, PharmD, PhD, for guiding me through the process of writing the thesis as well as the proofreading and his useful advice.

I would like to express my immense gratitude to Assist. Prof. Nika Lovšin, M. Chem., PhD, who accepted me to her research group, guided my lab work, provided me with much valuable advice and was always there for me to help.

I am grateful to Prof. Lucie Nováková, PharmD, PhD, and Assoc. Prof. Přemysl Mladěnka, PharmD, PhD, for the coordination of Erasmus+ Programme.

Last but not least, I would like to thank my family and friends for their overwhelming support.

Abstract

Charles University, Faculty of Pharmacy in Hradec Králové

Department of Pharmacology and Toxicology

Candidate: Josef Kunrt

Supervisor: Eduard Jirkovský, PharmD, PhD.; Assist. Prof. Nika Lovšin, M.Chem., PhD

Title of Diploma Thesis: Localisation of FUBP3 Protein in Human Cervical Cancer Cell Line

Osteoporosis is a skeletal disorder characterised by an impaired bone mass, strength and microarchitecture which leads to a higher risk of fracture. The disease is predominant in postmenopausal women but also affects older men and other risk groups, such as oncological patients.

To ascertain the genetic basis of osteoporosis, multiple genome-wide association studies have been performed with the aim to identify genes with a role in the diseases. These studies discovered multiple genetic loci associated with a higher risk of osteoporotic fractures, one of which was far upstream element-binding protein 3 (FUBP3). Works studying the properties of this protein such as cellular localisation are scarce. Therefore, we focused on establishing a protocol for visualisation of FUBP3 and its co-localization with other cellular structures in a human cervical cancer cell line (HeLa).

The visualisation was done using immunostaining of FUBP3 and GM130, a matrix protein of Golgi apparatus, and subsequent imaging with fluorescence microscopy. To confirm the immunostaining selectivity, we used shRNA mediated silencing of FUBP3 expression.

In this pilot study, we were able to successfully use immunofluorescence to visualise both FUBP3 and GM130 in HeLa cells as well as perform co-localization of both proteins at the same time. The established methodology will be utilized in further research in this field using another cellular model.

Abstrakt

Univerzita Karlova, Farmaceutická fakulta v Hradci Králové

Katedra farmakologie a toxikologie

Kandidát: Josef Kunrt

Školitel: PharmDr. Eduard Jirkovský, PhD.; Assist. Prof. Nika Lovšin, M. Chem., PhD

Název diplomové práce: Lokalizace FUBP3 proteinu v buněčné linii lidského cervikálního karcinomu

Osteoporóza je kostní choroba charakterizována narušením kostní hmoty, síly a mikroarchitektury, která vede ke zvýšenému riziku fraktury. Nemoc nejčastěji postihuje postmenopausální ženy, ale také starší muže a další rizikové skupiny jako jsou onkologičtí pacienti.

K zjištění genetického podkladu osteoporózy bylo provedeno několik pangenomických asociačních studií s cílem identifikovat geny, které by mohly hrát roli v tomto onemocnění. Tyto studie objevily několik lokusů spojených se zvýšeným rizikem osteoporotických zlomenin, z nichž jeden byl *far upstream element-binding protein 3* (FUBP3). O jeho významu a buněčné lokalizci však doposud existuje jen málo dostupných prací.. Z tohoto důvodu jsem se zaměřili na stanovení protokolu pro vizualizaci FUBP3 a jeho kolokalizace s dalšími buněčnými strukturami v buňkách lidského cervikálního karcinomu (HeLa).

Detekce proteinů FUBP3 a GM130, proteinu nacházejícího se v matrix Golgiho aparátu, byla provedena pomocí immunofluorescence s následnou vizualizací fluorescenčním mikroskopem. Pro potvrzení selektivity vazby protilátek na FUBP3 jsme provedli snížení exprese FUBP3 pomocí shRNA.

Výsledkem naší práce je úspěšné použití imunofluorescence ke zobrazení FUBP3 a GM130 v HeLa buňkách. Zároveň jsme byli schopni provést kolokalizaci obou proteinů v buňce. Stanovený protokol bude použit k následujícímu výzkumu na dalších buněčných modelech.

Table of contents

1. List of Abbreviations

AF	Alexa Fluor
ALP	alkaline phosphatase
ATP	adenosine triphosphate
BMD	bone mineral density
BSA	bovine serum albumin
cDNA	cyclic deoxyribonucleic acid
CMP	common myeloid progenitor
DKKK1	dickkopf-related protein 1
DMEM	Dulbecco's modified Eagle medium
EERα	oestrogen receptor-related receptor α
FBS	foetal bovine serum
FIR	FUBP interacting repressor
FRAX	Fracture Risk Assessment Tool
FUBP	far upstream element-binding protein
FUSE	far upstream element
GA	Golgi apparatus
GFP	green fluorescent protein
GWAS	genome wide-association study
hnRNA	heterogeneous nuclear ribonucleic acid
hnRNP K	heterogeneous nuclear ribonucleoprotein K
KH	K homology
LB	lysogeny broth
LBA	lysogeny broth with ampicillin

MSC	mesenchymal stem cells
NFATc1	nuclear factor of activated T-cells, cytoplasmic 1
NF-κB	nuclear factor κ-B
OCP	osteoclast precursor
OPG	osteoprotegerin
ORF	open reading frame
pAb	primary antibody
PBS	phosphate-buffered saline
pDNA	plasmid deoxyribonucleic acid
RANK	receptor activator of nuclear factor kappa-B
RANKL	receptor activator of nuclear κ-B ligand
sAb	secondary antibody
shRNA	short hairpin ribonucleic acid
siRNA	Short interfering ribonucleic acid
SNP	single nucleotide polymorphism
TFIIH	transcription factor of RNA polymerase II
Wnt	Wingless/Int-1

2. Introduction

The aetiology of osteoporosis and susceptibility to fractures is influenced by environmental aspects as well as genetic factors. Increased fracture risk is determined by an amalgamation of many biological processes in the musculoskeletal system.

Osteoporosis is a complex disease and studies targeting only a few genes are not enough to understand the minuscule influence of multiple gene variants on phenotype. That is the reason why genome-wide association studies (GWAS) were such a technological breakthrough not only for osteoporosis research. In two GWAS meta-analysis Far upstream element-binding protein 3 (FUBP3) was identified as a potential target of interest in the pathophysiology of osteoporosis. At the same time, the knowledge about its molecular function in regards to osteoporosis is very limited with only a few *in vitro* experiments done.

One of the first tasks to tasks on a way to understanding the function of FUBP3 in cells and later in osteoporosis is to localise the protein within the cell. This knowledge could provide us with hints about what functions the protein could possess.

3. Theoretical background

3.1. Epidemiology of osteoporosis

Osteoporosis is a skeletal disorder characterised by an impaired bone mass, strength and microarchitecture, which leads to a higher risk of fracture. It has a significant physical and psychosocial impact that affects not only the individual suffering from osteoporosis but also their family. On top of this, osteoporosis poses a financial burden for the healthcare and social system (NIH Consensus Development Panel on Osteoporosis Prevention, Diagnosis, and Therapy, 2001).

Osteoporosis can affect people of all age groups, genders and races, although postmenopausal women, elderly and individuals with European heritage are more prone to develop osteoporosis during their lives. It was estimated that 40 % of white postmenopausal women are affected by osteoporosis and the incidence is predicted to be continuously increasing with the ageing population (Cole et al., 2008; Reginster and Burlet, 2006).

A significant complication of osteoporosis is fractures. The risk of a fracture in a patient with osteoporosis can be as high as 40 %. Fractures of vertebras, hip or wrist are the most common, but other bones such as the trochanter, humerus or ribs can also be affected. The first two mentioned osteoporotic fractures are carrying the biggest elevation in 12-month mortality because they often require hospitalisation and as a result, they increase the risk of other complications such as pneumonia or thromboembolic disease due to prolonged immobilisation of the patient as the recovery can be slow and incomplete (Center et al. 1999). In 2010, it was estimated that 43 000 deaths were related to osteoporotic fractures (Svedbom et al., 2013).

The same study also estimated the economic burden of the incident and prior fragility fractures at 37 billion euros in 27 EU countries. It is expected that the cost will increase by 25 % in 2025 (Svedbom et al., 2013).

3.2. Diagnosis of osteoporosis

Osteoporosis is generally under-diagnosed as the slow bone loss is initially asymptomatic and the first signal for diagnosis is often when the first clinical fracture occurs (Vestergaard et al., 2005). Therefore, targeted risk assessment is crucial for correct and timely diagnosis of osteoporosis. According to the National Institute for Health and Care Excellence (2017) in the United Kingdom, the assessment should be done in all women aged over 65 years and all men aged over 75 years. For individuals below this age, routine assessment is not needed unless there are risk factors present such as previous fragility fracture, current use or frequent recent use of oral or systemic glucocorticoids, history of falls, family history of hip fracture, other causes of secondary osteoporosis (e.g. certain malignancies), low body mass index, smoking or alcohol intake of more than 14 units per week (the equivalent of six beers or seven glasses of wine).

The diagnosis itself relies on the quantitative assessment of bone mineral density (BMD). It can be measured with densitometric techniques in vivo. Dual-energy ray absorptiometry is the most used technique. For clinical practice, BMD is converted to T- or Z-score. Both of these parameters represent the units of standard deviation difference with the reference BMD value. A T-score shows the standard deviation by which BMD of an individual differs from the mean of a healthy 30-year old adult of the same sex. A Z-score is the same as T-score except the standard deviation by which BMD differs is the mean BMD value expected in an individual of the same age and sex (Kanis et al., 2019). According to the World Healthcare Organization, values of T-score between -1.0 to -2.5 SD show low bone mass. Values below -2.5 SD is the definition of osteoporosis with a lower number meaning that the severance of osteoporosis is increasing (Bounjour et al., 2004).

Unfortunately, BMD alone captures the risk of future fracture imperfectly. Moreover, a normal BMD measurement is no guarantee that a fracture will not occur. For this reason, a Fracture Risk Assessment Tool (FRAX) has been developed. Beside BMD, it takes into account age and sex as well as other skeletal and non-skeletal factors that have an impact on fracture risk. It estimates the ten-year probability of clinical major fracture and/or hip fracture. Since risk factors are dependent on geographical location, FRAX is calibrated for individual countries (Kanis et al., 2008).

3.3. Current therapies of osteoporosis

Before any pharmacological therapy is employed changes to lifestyles such as giving up of smoking, reduction of alcohol intake and increased physical activity are advised to the patient. Supplements containing vitamin D and calcium are recommended to every osteoporosis patient. The efficacy of specific osteoporosis drugs has only been shown if these supplements were concurrently given. A usual dose of vitamin D is at least 800 UI per day (Holick, 2007).

Pharmacological therapies of osteoporosis can be divided into two classes. First are antiresorptive drugs, which slow down the bone resorption and the second are anabolic drugs, that promotes bone formation.

In the group of antiresorptive medicines, bisphosphonates such as alendronate, risedronate and zoledronate are the golden standard as they have a high affinity for bone and long history of safe use. The usual route of administration is peroral, but bisphosphonates can be also administered intravenously. Other advantages are their low price and possible use across a broad spectrum of osteoporosis types (e.g. postmenopausal, steroid-induced or male-type). Other drugs in this group pose an alternative for postmenopausal women, and representatives are raloxifene, a selective estrogen receptor modulator, calcitonin, a peptide hormone that lowers the blood calcium level and most recently denosumab, a monoclonal antibody against receptor activator of nuclear factor-kappa B ligand (RANKL) (Chen and Sambrook, 2012).

Bone-anabolic drugs are in comparison to antiresorptive medicines a smaller group of medicines. There are two clear anabolic drugs for the treatment of osteoporosis available at present. First is full length human recombinant parathyroid hormone (PTH 1-84), approved for use in Europe, and second is recombinant N-terminal fragment parathyroid hormone (PTH 1-34, teriparatide), which is approved for use in Europe and USA. Indication of both PTH 1-84 and teriparatide is postmenopausal osteoporosis, male osteoporosis and steroid-induced osteoporosis. Both have to be administered as subcutaneous injections daily for up to two years (Mosekilde et al., 2011).

Strontium ranelate is another medicine used in the therapy of osteoporosis. According to several studies, it has a dual effect on the bone as it is simultaneously decreasing bone resorption and increasing bone formation (Bonnelye et al., 2008; Marie et al., 2011).

3.4. Bone biology

During the past decade, scientists have linked the pathogenesis of osteoporosis to tissue, cellular and molecular processes. At the cellular level, the communication and coupling between osteoblasts, bone-forming cells, and osteoclasts, bone-degrading cells, is regulated and coordinated by several key molecules, which are essential for keeping a balance during bone remodelling. These molecules are influenced by so-called master signals, that integrate various endocrine, neuroendocrine, inflammatory and mechanical stimuli.

The cycle of bone turnover starts with lining cells of the endosteal surface being retracted. The endosteal collagenous membrane is digested by matrix metalloproteinases revealing the bone itself for osteoclasts. Subsequently, osteoblasts enter the resorption cavity and create new osteoid which later calcifies. This process is completed in approximately 3-6 months (Datta et al., 2008).

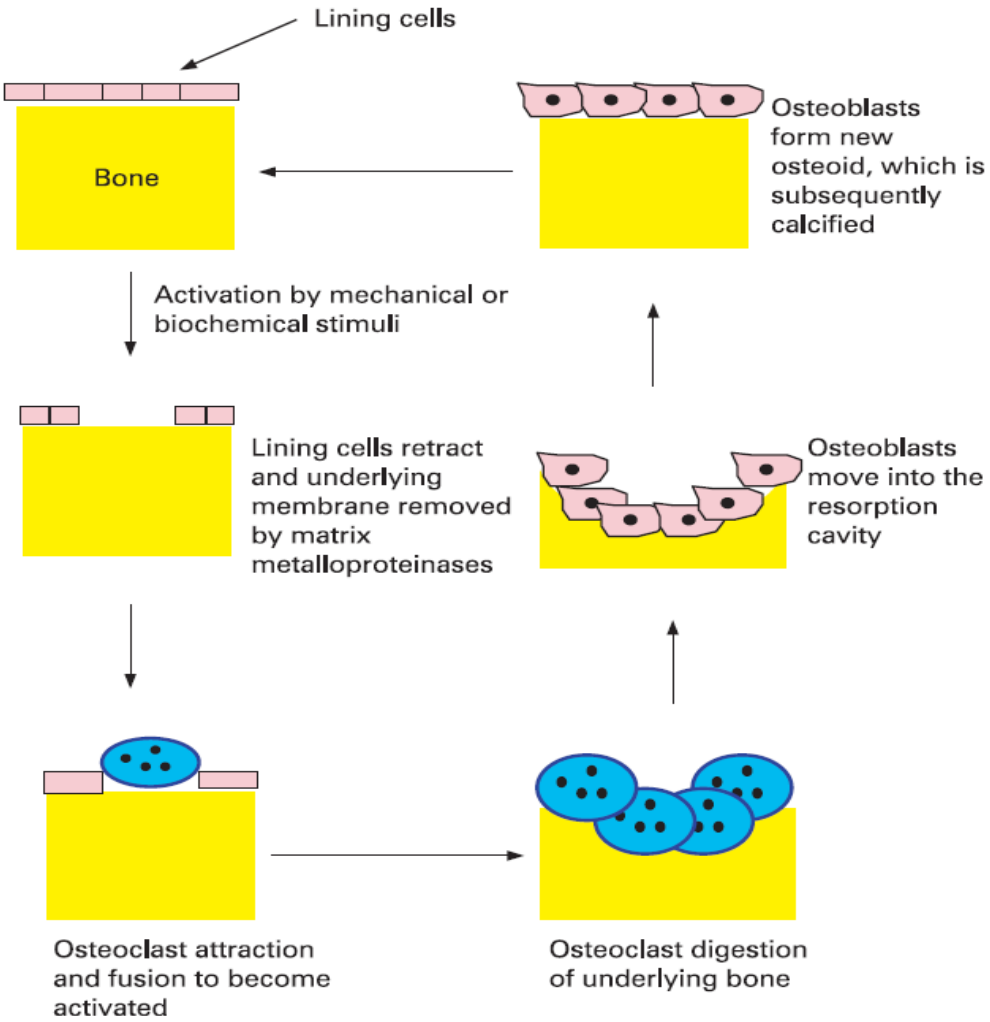

Figure 1: Osteoblast and osteoclast activities in the cycle of bone turnover. (Taken from Datta et al. 2008)

3.4.1. Osteoclasts and bone resorption

Osteoclasts are non-dividing, multinuclear bone-resorbing cells, that arise from hematopoietic stem cells, more precisely from common myeloid progenitor (CMP) in the myeloid pathway (Athanasou and Quinn, 1990).

Early differentiation when hematopoietic stem cell proliferates within macrophage lineage up to osteoclast precursor (OCP) is dependent on transcription factor PU.1, microphthalmia transcription factor (MITF) and macrophage-colony stimulating factor (M-CSF). OCP commit to becoming osteoclast under the influence of RANKL and subsequently undergoes fusion with several other osteoclasts to form the multinuclear polarized cell (Soysa et al., 2012).

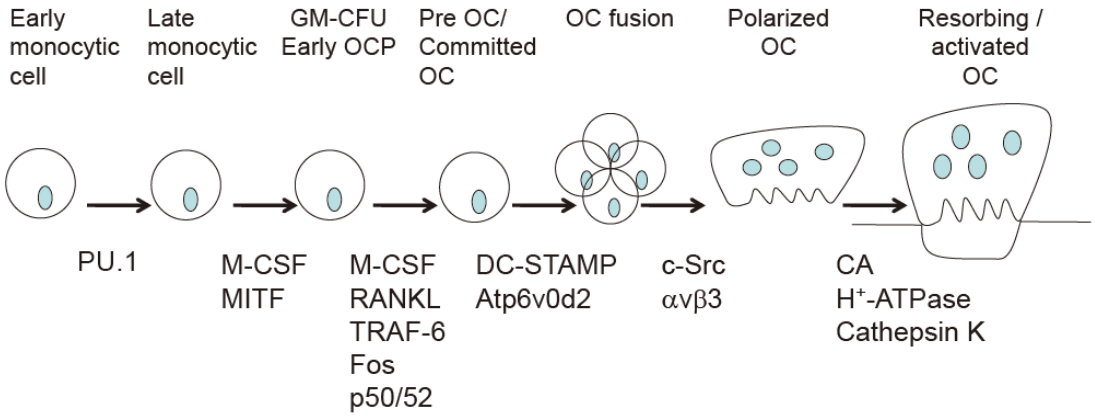

Figure 2: Regulation of osteoclast formation and differentiation. (Taken from Soysa et al. 2012)

The polarized osteoclast represents the „bone-resorbing unit“ which attaches to the bone, initiating the bone degradation. The cell creates a ruffled membrane and seals off a part of a bone generating an isolated extracellular microenvironment, which is required for bone resorption. Integrins, especially $\alpha_v\beta_3$ integrin, play an essential role in the process of resorption. It is responsible for the regulation of cell adhesion of osteoclast and osteoclastic migration (Nakamura et al., 2007).

The process of bone resorption starts with the inorganic phase of the bone being dissolved in an acidic environment mediated by a vacuolar H^+-ATPase. The intracellular pH is maintained by an energy-dependent Cl^- /HCO_3^- exchanger on the opposite side to the

resorptive surface. For the function of both transporters, carbonic anhydrase II catalyse the generation of H^+ and HCO_3^- from CO_2 created via cellular respiration. The electroneutrality of intracellular environment is achieved by Cl^- channel, charge-coupled to the H^+-ATPase. These ion transporting events result in the secretion of HCl into the resorptive cavity, creating a pH of approximately 4.5. The demineralized organic matrix is subsequently degraded by a liposomal protease, cathepsin K. Dissolved bone matrix is endocytosed by the osteoclast and transported to and released at the antiresorptive surface (Teitelbaum, 2000).

Osteoclasts not only act directly by resorbing bones but also regulate functions of osteoblasts positively and negatively. They also play a role in the release of hematopoietic cells from the bone marrow in the bloodstream and influence immune response in pathological states. (Boyce et al., 2009).

3.4.2. RANKL-RANK-OPG pathway

Genetic experiments showed that activator of nuclear factor κ-B ligand (RANKL), receptor activator of NF-κB (RANK) and decoy receptor osteoprotegerin (OPG) are essential regulators of osteoclast function and bone homeostasis. RANKL, RANK and OPG are members of the tumour necrosis factor (TNF) and TNF receptor superfamilies.

RANKL is a protein consisted of C-terminal extracellular receptor-interacting domain and transmembrane domain. By proteolytic cleavage from the membrane-embedded portion, a soluble form of RANKL is created. RANKL expression has been detected in T lymphocytes, osteoblasts, osteocytes and bone stroma, and lung tissue. Expression of RANKL can be induced by various factors such as glucocorticoids, vitamin D3, interleukin-1, TNF-α, TGF-β, Wnt ligands and lipopolysaccharide. RANKL binds to both RANK and OPG (Walsh and Choi, 2014).

Receptor activator of NF-κB (RANK) is the signalling receptor for RANKL. It is a transmembrane protein composed of homo-trimerizing membrane domain and four extracellular cysteine-rich pseudorepeats. RANK is expressed by various cells such as OCPs, mature osteoclasts and dendritic cells but also mammary glands. It is also expressed by some cancer cells, including breast and prostate, and it might have a role in tumour cell proliferation (Boyce and Xing, 2008).

RANK is connected to a complex downstream signalling pathway as it lacks intrinsic kinase activity. Activated RANK is associated with tumour necrosis factor receptor-associated factors (TRAFs) 1,2,3,5 and 6. Among those TRAF6 plays, a major role in osteoclasts functions as it is activating mitogen-activated protein kinases (MAPKs), p38 and c-Jun N-terminal kinase 1 which are involved in osteoclastogenesis. TRAF6 is also essential for activation of canonical NF-κB pathway which is needed for osteoclast development and osteoclast function (Wada et al., 2006).

Other adaptor and docking proteins that may modulate RANK signalling include Grb2-associated binding protein (Gab2), epidermal growth factor (EGFR), four-and-a-half LIM domain 2 (FHL2), Lyn, CYLD de-ubiquitinase and TRAF family member associated NF-κB activator (TANK). Ultimately it induces the transcription factors c-fos, nuclear factor of activated T-cells, cytoplasmic 1 (NFATc1), NF -κB members p50 and p52. These transcription factors activate the transcription of osteoclast-critical genes for the expression of tartrate-resistant acid, cathepsin K, calcitonin receptor as well as c-myc, that is important in the promotion of osteoclast proliferation. RANKL-RANK is also essential for functioning bone resorption by mature osteoclast as it activates Src-dependent pathways as it promotes the formation of the ruffled membrane (Walsh and Choi, 2014).

Osteoprotegerin is disulfide-linked homodimer protein secreted by various cell types in addition to osteoblasts, including bone marrow stromal cells, B lymphocytes, dendritic cells and follicular dendritic cells. Expression of OPG is tightly connected to inductors and inhibitors associated with bone homeostases, such as TGF-β, IL-1, TNF-α, oestrogen, Wnt ligands and glucocorticoids. It is believed that OPG main function is to pose as a soluble decoy receptor for RANKL and thus serving as a negative regulator of RANK signalling. Other potential physiological relevant ligands include syndecan-1, glycosaminoglycans, von Willebrand Factor and Factor VIII von Willebrand Factor complex (Walsh and Choi, 2014).

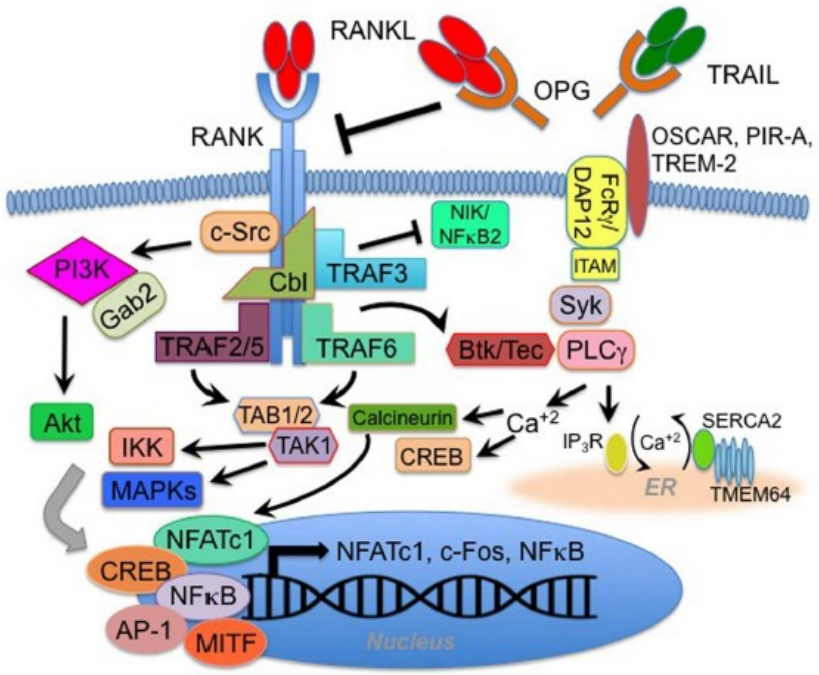

Figure 3: RANK signalling pathway (Taken from Walsh a Choi 2014)

3.4.3. Osteoblasts and bone formation

Osteoblasts are terminally differentiated single nuclear cells. They arise from mesenchymal stem cells (MSC) which are pluripotent cells with located in bone marrow, periosteum, vessel walls, muscle and circulation. They have the potential to differentiate into a limited number of cell types. Differentiation of MSC to particular cell lineage is dependent on several growth factors (Kratchmarova et al., 2005).

One of the vital roles of MSCs is in initial bone formation as they are the precursor for chondrocytes, that lay down cartilage which is later calcified and remodelled into the bone in a process called endochondral ossification (Dimitriou et al., 2005).

The differentiation of osteoblasts and chondrocytes is connected as they have a common precursor called osteochondroprogenitor. There are several transcription factors essential for the differentiation such as Runx2/Cbfa1, Sox9 and osterix (Heino and Hentunen, 2008). Osteoblasts are also connected to adipocytes through common progenitor and through osteoblast-adipocyte transdifferentiation, which plays a role in the balance of bone formation and bone marrow adipogenesis (Park et al., 1999).

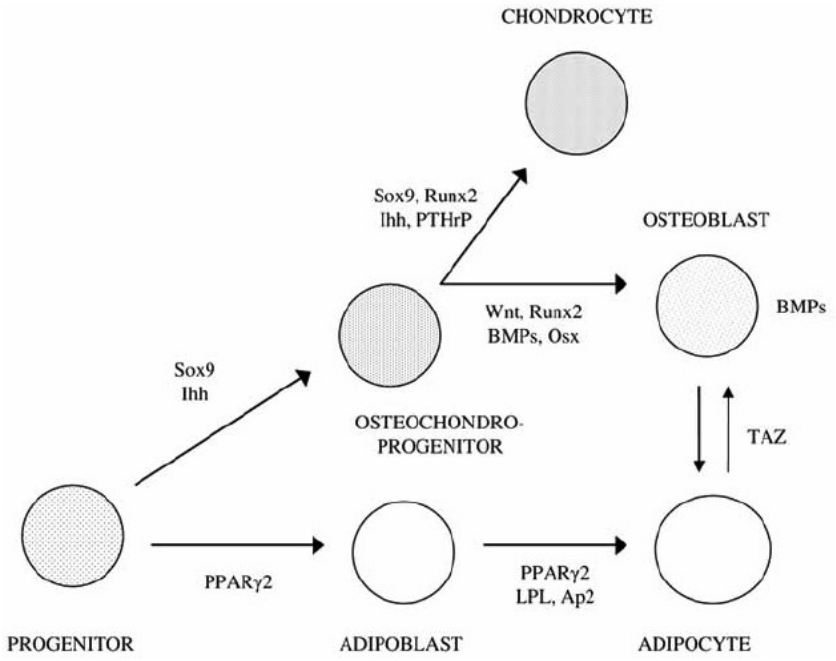

Figure 4: Simplified schema of chondrocyte derivation from MSC-progenitor cells. (Taken from Heino a Hentunen 2008)

Fully differentiated osteoblasts have cuboidal shape, prominent Golgi apparatus and well-developed endoplasmic reticulum. The process during which osteoprogenitor becomes osteoblast consists of three main stages. Right after the proliferation stage, type I collagen and non-collagenous proteins are produced, creating the organic bone matrix. Expression of alkaline phosphatase (ALP), a membrane-bound enzyme, follows the production of type I collagen and it is the highest immediately before the third stage, mineralization. (Aubin, 1998). The process of mineralization is dependent on ALP and is different in a lamellar and woven bone. Calcium and phosphate ions are deposited into the organic matrix making rigid and impenetrable. The osteoblasts are therefore trapped within the matrix and either die or differentiate into osteocytes.

It is hypothesised that bone lining cells are descendants of MSCs (Parfitt, 1994). These cells make up often multiple layers that cover bones that are not undergoing remodelation. There is not much knowledge about their origin, proliferation, differentiation and function, although there are several hypotheses. The cells itself are extremely flat, with few organelles (Miller et al., 1980).

Another important process in bone formation is angiogenesis. Many angiogenic growth factors such as fibroblast growth factors (FGFs) and vascular endothelial growth factors (VEGFs) have a role in bone formation and repair (Heino and Hentunen, 2008).

3.4.4. Wnt pathway

Wingless/Int-1 (Wnt) signalling pathway is made up of a family of 19 secreted signalling glycoproteins, that plays a role in plenty of processes, such as cell proliferation, differentiation, apoptosis, survival, migration and polarity in many of cell types. Wnts are crucial in organism since embryonic development (Kikuchi et al., 2009).

The Wnt proteins are secreted from cells in very hydrophobic form due to covalently bound palmitate. Enzymatic removal of palmitate results in loss of activity, which suggests that palmitoylation is important for Wnt signalling (Johnson et al., 2004).

There are also several Wnt receptor, the main being low-density lipoprotein receptor-related protein (LRP) 5, LRP6 and frizzled receptor family. LRP5/6 are single-pass transmembrane proteins (Tian et al., 2003). The frizzled proteins are seven-transmembrane serpentine receptors. The extracellular portion serves as a ligand-binding unit while the transmembrane part is the signalling portion of the protein (Malbon, 2004). Both LRP5/6 and frizzled proteins are needed for activation of the signalling pathways because they work as co-receptors.

Different Wnt receptors bind a different set of Wnts and as a result, selectively activating distinct intracellular signalling pathways. There are three different intracellular pathways activated by different pairs of Wnts and Wnt receptors: the Wnt/β-catenin pathways (also known as the canonical Wnt pathway), the non-canonical Wnt pathway and the Wnt-calcium pathway.

The canonical Wnt pathway is the main regulation mechanism of osteogenesis, along with bone morphogenetic proteins. Osteoblast differentiation is dependent on the presence of β-catenin. In its absence, the mesenchymal cells do not differentiate into osteoblast but rather follow the path towards chondrocytes. It also promotes the differentiation of osteoblast by suppressing adipogenesis (Rossini et al., 2013). In particular, the canonical pathway promotes the progression of osterix-expressing cells to osteoblasts. Wnts also prevent apoptosis of mature osteoblast and thus prolonging their lifespan

(Almeida et al., 2005). The Wnt/β-catenin pathway also inhibits the differentiation of osteoclasts by promoting the production and secretion of OPG (Glass et al., 2005).

The regulation of the canonical pathway in bone is mediated by the production of Wnt receptors‘ inhibitors such as sclerostin (SOST) and dickkopf-related protein 1 (DKK1) (Rossini et al., 2013).

The non-canonical Wnt pathway is tight to osteoclast differentiation. It was reported that Wnt16 which activates the canonical pathway also activates the non-canonical pathway in osteoclast precursors. There, it suppresses the RANKL-induced activation of Nf-κb and NFATc1 (Kobayashi et al., 2018).

3.4.5. Osteocytes

Osteocytes are the most abundant cells of mammalian bones. It was estimated that there are ten times more osteocytes than osteoblasts in an individual bone.

When osteoblasts finish their role as bone-forming cells, three main fates are waiting for them. They will either undergo apoptosis, transform into inactive osteoblasts and become bone-lining cells or become embedded in the bone as osteocytes. Once is osteoblast embedded in the bone matrix, it ceases its activity as bone-forming cells, but gain many new functions. This highly complex phenotypic transition is orchestrated by several molecular mechanisms (Franz-Odendaal et al., 2006).

The cells undergo a dramatic change in shape, from cuboidal to dendritic cells with a small body and numerous long, slender processes that connect to nearby osteocytes as well as osteoblasts and bone-lining cells on the surface of the bone. This network of osteocytes and their processes can be seen even on a microscopic level as lacunae, holes in the bone matrix where osteocytes reside, and canaliculi, channels around osteocytes‘ processes, are the most prominent morphological feature of bones (Palumbo et al., 1990).

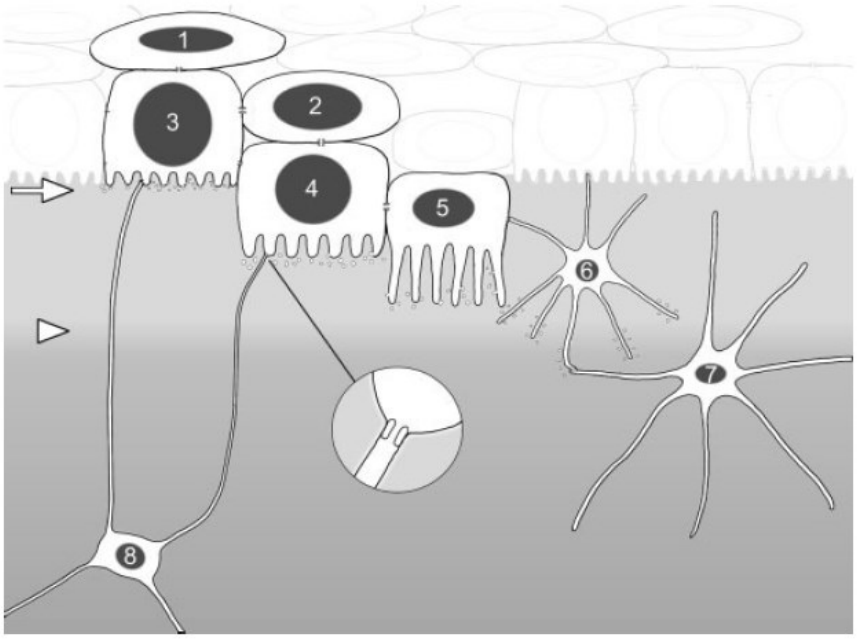

Figure 5: Diagram showing the transitional cell types between preosteoblasts and osteocytes during osteoblast. 1. preosteoblast, 2. preosteoblastic osteoblast, 3. osteoblast, 4. osteoblastic osteocyte (Type I preosteocyte), 5. osteoid-osteocyte (Type II preosteocyte), 6. Type III preosteocyte, 7. young osteocyte, 8. old osteocyte. (Taken from Franz-Odendaal et al. 2006)

The pericellular space within the lacunar-canalicular system serves as a connection with the outer environment, providing the cells with nutrients and waste removal, as well as enabling the cells to communicate with each other, and other cells within the bone. Osteocytes produce many different molecules such as non-collagenous proteins, proteoglycans, hyaluronic acid and several cytokines (Schaffler et al., 2014).

Osteocytes serve as a bone mechanosensors and mechanotransductors. Several proposed stimuli can be sensed by osteocytes, including physical deformation of the bone itself, the load-induced flow of fluid through the lacunar-canalicular system which results in fluid flow shear stress, or changes of electrical potential (as the fluid is an ionic solution) along the charged surfaces of lacunocanalicular wall and/or cell membrane of osteocytes (Weinbaum et al., 1994).

The communication among osteocytes is crucial for effective integration of local and global stimuli. At the same time, osteocytes have to communicate with the surface bone cells to relay the stimuli from inside the bone to osteoblast and osteoclast, which play a role in bone

remodelation. Both direct and indirect means of communication are employed (Schaffler et al., 2014).

Direct communication is done via gap junctions and connects not only osteocytes to osteoblasts and bone lining cells but also endothelial cells of bone capillaries. Indirectly osteocytes are communicating via paracrine signalling transduced by small metabolites, such as prostaglandins, nitric oxide (NO), and ATP. Hemichannels and pannexin channels play a role in this type of communication. Paracrine signalling can be also transduced by macromolecules, like sclerostin and RANKL, which are produced by osteocytes and parathyroid hormone for which osteocytes express receptors (Schaffler et al., 2014).

Osteocytes have an activating effect on osteoblasts when a bone is exposed to mechanical stress. This activation is done via prostaglandins, cyclic adenosine monophosphate and NO. Inhibitory effect of osteocytes on osteoblasts is through the production of sclerostin, an antagonist of canonical Wnt signalling pathway, and DKK1 another inhibitor of this pathway. Mechanical loading of bone decreases expression of both sclerostin and DKK1 resulting in increased bone formation. Unloading of bone acts in the opposite manner, it increases expression of both mentioned proteins, and thus inhibits bone formation (Bonewald and Johnson, 2008).

The effect of osteocytes on osteoclasts is not as straightforward as in the case of osteoblasts. Data from several studies suggest that osteocyte apoptosis is a principal trigger for osteoclast resorption. The proposed mechanism of action is following apoptotic osteocytes, usually in the centre of microcracks, send a signal, so far unknown, to neighbouring osteocytes which start to express active antiapoptotic response as well as upregulate expression of RANKL and downregulate the expression of OPG (O'Brien et al., 2013).

3.5. Genetics of osteoporosis

Several key mechanisms in bone biology were identified by studies of rare monogenic bone disorders. The importance of bone collagen matrix quality was shown in the study of osteogenesis imperfecta. Signalling pathways such as Wnt, Notch and RANK-RANKL-OPG were identified in studies focused on Van Buchem disease, Hajdu-Cheney syndrome and autosomal recessive osteopetrosis. The crucial role of cathepsin K in osteoclast

function was to discover while studying pycnodysostosis (Rocha-Braz and Ferraz-de-Souza, 2016).

3.5.1. C-*myc* and its role in osteoporosis

C-*myc* belongs to *myc* family of genes which all are a part of a group of protooncogenes and regulator genes. It plays a critical role in cell proliferation as shown in several studies. Targeted deletion of c-*myc* in mice caused embryonic lethality (Davis et al., 1993). Rat fibroblast cell line with disruptions of both c-*myc*gene copies had prolonged cell doubling time (Mateyak et al., 1997). It was estimated that c-*myc* regulates expression of around 15 % of all genes through the binding on enhancer box sequences (Gearhart et al., 2007). C-*myc* also plays a role in the process of apoptosis (McMahon, 2014).

From the structural point of view, c-*myc* is located on human chromosome 8, organized into three exons, encoding multiple transcription variants which are generated not only by variable usage of transcriptional start sites and polyadenylation signals but also alternative mRNA processing. Both 5‘ and 3‘ end contains large untranslated regions which are unique for each *myc* family member. C-*myc* , as well as the rest of the family, contains a basic helix-loop-helix motif, which allows binding to DNA, and leucine zipper motif, which allows dimerization with other transcription factors (DePinho et al., 1991).

A study done by Battaglino et al. 2002 focused on determining the role of c-*myc* in osteoclast differentiation from its precursors. They used mouse monocytes as a model system for osteoclast differentiation. The cells were induced by with RANKL and formed OCLs which expressed typical osteoclast markers and were functioning as osteoclasts on calcium phosphate films and bone slices. C-*myc* was strongly up-regulated in RANKL-induced OCLs. On the other hand, it was absent in undifferentiated cells. The study concluded that c-*myc* is a downstream target of RANKL and its expression is required for RANKL-induced differentiation of osteoclasts.

On top of this Bae et al. 2017 ascertained that c-*myc* on top of previously established linked between c-*myc* expression and osteoclastogenesis functions as a metabolic switch to oxidative stress. They also aimed to find where exactly in the RANKL signalling pathway c-*myc* plays a role. They concluded that c-*myc* has the role of a transcriptional inductor of oestrogen receptor-related receptor α (EERα), that cooperates with NFATc1 in osteoclastogenesis. The findings were supported by an experiment with pharmacological inhibition of ERRα, which protected ovariectomized rats against bone loss.

3.5.2. Far upstream element-binding protein family

Far upstream element-binding protein (FUBP) family is a group of single-strand DNA-binding proteins with features putting them in the category of transcription factors. As the name suggests, the proteins bind to far upstream element (FUSE), which is located approximately 1.5k bp upstream of the transcription start site in the promoter region, that is required for maximal transcription of c-*myc*. FUBP is present in extracts of undifferentiated cells but disappears upon differentiation (Avigan et al., 1990). As a result FUSE and FUBPs are contributing to the regulation of cell proliferation and differentiation.

The structure of FUBP is comprised of three distinct domains: amino-terminal, central and carboxyl-terminal. The central domain which is crucial for single-strand DNA binding and sequence recognition consists of four evenly spaced unit which is made of a 30-residue direct repeat and amphipathic helix separated by 18 to 21 residues. The third and fourth repeat helix unit are needed to constitute a DNA-binding domain. FUBPs bounds preferentially to the noncoding strand of the FUSE site as a single-stranded oligonucleotide (Duncan et al., 1994).

The pattern of repeats and helices is unique for FUBP family and does not resemble any known DNA-binding motif. However, the repeats alone are similar to K homology (KH) motif in heterogeneous nuclear ribonucleoprotein K (hnRNP K), an RNA-binding protein which makes complexes with heterogeneous nuclear RNA (hnRNA) (Siomi et al., 1993).

Although initially it was not believed that FUBP binds to RNA even though the KH motif, several subsequent studies showed FUBP1 binds to different cellular and viral mRNAs. Zheng and Miskimins (2011) showed that FUBP1 binds to p27 mRNA 5‘ untranslated region and promotes an internal ribosome entry site which activates its translation. Olanich et al. (2011) proposed that FUBP1 is a regulator of cell growth and proliferation through the ability to selectively bind to 3‘ untranslated region of nucleophosmin, a multifunctional oncoprotein, and represses its translation. Chien et al. (2011) found out that FUBP1 binds to 5‘ and 3‘ untranslated regions of Japanese encephalitis virus (JEV) genome and supresses the JEV’s proteins expression. The team proposes that FUBP1 functions as part of JEV defence system.

A study done by Vindigni et al. (2001) showed that FUBP1 is identical to novel human helicase, HDH V, found in HeLa cells. FUBP1 unwinds DNA with a 3‘ to 5‘ polarity and needs ATP for its functioning. It can only unwind short (17 bp) duplex DNA molecules, which suggests that FUBP is not a processive enzyme. Since FUBP does not bind to double-stranded DNA the DNA helix in the position of FUSE may be partially unwound due to being localized in a region of helical instability.

This hypothesis was further investigated by Liu et al. (2006) to determine if in vitro observed melting of FUSE by transcriptionally generated torsion and subsequent FUBP/FUBP Interacting Repressor (FIR) regulation of c-myc transcription happens in vivo as well. In this hypothesis, it is assumed that FUSE poses as mechanoreceptor whereas FUBP/FIR are the effectors. The study results suggest following the mechanism of transcription at the c-myc promoter. In the beginning, one or more transcription factors that respond to initial stimulus binds to c-myc promotor. This starts a cascade of events during which the chromatin remodels and along with torsional stress caused by the moving polymerase causes melting of FUSE. This process allows FUBP to bind to FUSE and act as a second-stage booster of transcription which results in fully melted FUSE. This allows FIR to come into play, slowing down the transcription, lowering the dynamic stress and consequently ejecting FUBP but not FIR. FUBP and FIR along with TFIIH, a transcription factor of RNA polymerase II, tune the activity of c-*myc* in pulses.

Since c-*myc* is involved in cell differentiation, proliferation and apoptosis and FUBP is involved in c-*myc* regulation, it is not surprising that FUBP, more precisely FUBP1, is implicated in multiple types of cancer such as oligodendrogliomas, non-small cell lung cancer, breast, clear cell renal cancer, liver, colon, bladder and prostate. The fact that FUBP1 expression in normal cells is low and high in tumour tissues it is also proposed as a potential biomarker for these types of cancers (Zhang and Chen, 2013).

3.5.3. Current knowledge about FUBP3 and its connection to osteoporosis

FUBP3 is probably the least studied member of FUBP family. It was described by Davis-Smyth et al. (1996) in a study focused on cloning and expression of FUBP2 and FUBP3 cDNAs. The FUBP3 cDNA is composed of 3169 nucleotides which encode 600 amino acids ending with TAG at nucleotide 1809. The open reading frame (ORF) of FUBP3 is in between ORF of FUBP1 and FUBP2 with respect to preferential utilization of

uncommon codons. The general structure of the protein family is preserved. The amino acid sequence of FUBP3 is further from FUBP2 than FUBP1 suggesting that FUBP1 is the oldest member of the protein family. Experiment in promonocytic leukaemia cell line U937 and promonomyelocytic leukaemia cell line HL60 showed that FUBP3 mRNA does not disappear after differentiation.

The gene for human FUBP3 is localized on chromosome 9, in chromosome band 9q33-34.1 (Bouchireb and Clark, 1999). Functions of FUBP3 have been only poorly described. As mentioned previously, FUBP3, as well as other members of FUBP family, might have a role in certain kinds of cancer. Weber et al. (2008) studied FUBP1, FUBP3 and c-*myc* expression in renal cell, prostate and urinary bladder carcinomas. Both FUBPs were expressed in high rates in all cancer types. High FUBP1 and FUBP3 expression associated with c-*myc* up-regulation was significant only in the case of clear cell renal carcinomas, but neither in bladder nor prostate cancer which means that both FUBPs are potential c-*myc* regulators in renal cancer.

The use of genome-wide associations studies (GWAS) in osteoporosis research has significantly expanded knowledge about the possible genetic causes of this disease. GWAS is hypothesis-free screening looking for single nucleotide polymorphisms (SNPs) that occur more frequently in people suffering from the particular disease (Visscher et al., 2012).

The largest GWAS meta-analysis done by Estrada et al. 2012 in the field of osteoporosis successfully identified 56 bone mineral density loci, of which 14 were also associated with elevated risk for osteoporotic fractures. Subsequent GWAS meta-analysis done by Trajanoska et al. 2018 identified 15 fractures associated loci. All of the identified loci were associated with bone mineral density.

In both of these GWAS meta-analyses (Estrada et al., 2012; Trajanoska et al., 2018) was *FUBP3* identified as a locus associated with bone mineral density and osteoporotic fracture risk. A study done by Gau et al. (2011) investigated the possible interacting proteins binding to TG microsatellite in the 3‘ untranslated region of *FGF9* mRNA, which was previously shown as a place for modulation of FGF9 expression. During the experiments, upregulation of FGF9 was observed as a response to transient overexpression of FUBP3. When the expression of FUBP3 was halted in knockout HEK293 cells, the expression of FGF9 was downregulated as well. These results were confirmed by subsequent experiments. To put the findings in the context of osteoporosis, FGF9 is required for angiogenesis and

osteogenesis in long bone repair (Behr et al. 2010). This could suggest that SNPs in *FUBP3* might diminish its expression and through this influence the expression of FGF9.

Therefore, FUBP3 seems to be a promising candidate for osteoporosis diagnosis marker.

4. Aim of the work

We aimed to establish a protocol for overexpression of FUBP3 protein in HeLa cells, its further immunofluorescent detection along with its co-localization in Golgi apparatus and establishing a protocol for silencing of FUBP3 expression with shRNA.

We will test the following hypothesis:

1. FUBP3 is primarily located in the nucleus as it is probably the main place of action of the protein.
2. The secondary localisation of FUBP3 is in the Golgi apparatus where it is stored before release to the cytoplasm.

5. Materials and methods

5.1. Chemicals and reagents

Chemicals:

- Agarose (Fluka Analytica)
- Antibiotic/antimycotic (Biowest)
- Ampicillin (Sigma Aldrich)
- Dulbeccos‘ modified medium (DMEM) (Biowest)
- 10x Phosphate buffer solution (Sigma Aldrich)
- Foetal bovine serum (Biowest)
- PolyJet DNA InVitro Transfection (SignaGen Laboratories)
- Trypsin (Biowest)
- 4% Paraformaldehyde
- Bovine serum albumin (Sigma Aldrich)
- Skim milk (Merck)
- Invitrogen ProLong Gold Antifade Mountant with DAPI (ThermoFisher Scientific)
- Trypan Blue (Sigma Aldrich)
- QIAprep Spin Miniprep Kit (QIAGEN)
- PureYield Plasmid Midiprep (Promega)

Antibodies:

- Anti-FLAG M2 produced in mouse (F3165; Sigma Aldrich)
- Anti-FUBP3 produced in mouse (sc-398466; Santa Cruz Biotechnology)
- Anti-GM130 produced in rabbit (G7295; Sigma Aldrich)
- Anti-mouse IgG Alexa Fluor 555 (A31570; Thermo Fisher Scientific)
- Anti-rabbit IgG Alexa Fluor 488 (A11008; Thermo Fisher Scientific)

Plasmids:

- pCMV-FLAG-FUBP3 (created at the Faculty of Pharmacy, University of Ljubljana, unpublished)
- FBP3 shRNA Plasmid (h) (sc-106747-SH; Santa Cruz Biotechnology)
- Control shRNA Plasmid-A (sc-108060, Santa Cruz Biotechnology)

Cell lines:

- HeLa
- DH5alpha competent cells

5.2. Production of pCMV-FLAG-FUBP3 plasmid

5.2.1. Transformation of DH5alpha competent cells

Cell transformation is a process during which competent cells directly uptake and incorporate exogenous genetic material from its surroundings through the cell membrane. For our experiments, we have chosen DH5alpha *E. coli* competent cells. They are *E. coli* strain designed to be suitable for transformation. The process during which the cells gain competence makes them vulnerable to sudden changes in external conditions and they must be handled with care.

DH5alpha competent cells were thawed on ice and 1 µl of pCMV-FLAG-FUBP3 plasmid was aseptically pipetted into the tube with bacteria. All tubes were incubated for 30 minutes in ice. After the incubation the cells were exposed to heat shock of 42°C for exactly 45 seconds, followed by immediate transfer of the tubes on ice for 60 seconds. Each tube was diluted with 500 µl of lysogeny broth (LB) liquid medium and incubated in 37°C on the shaking plate for 1 hour. After the incubation, 50 µl of bacteria were plated on LB plates with added ampicillin (LBA) as a selection factor. Plates were covered with aluminium foil to prevent drying and incubated overnight at 37°C.

Following the overnight incubation, colonies of bacteria were noticed. One colony was aseptically transferred to 3 ml of LBA liquid medium and incubated overnight at 37°C with shaking. Plates itself were covered with parafilm to prevent future drying and stored at 4°C.

5.2.2. Plasmid DNA isolation using DNA-binding silica column

Plasmid DNA was isolated from overnight culture using QIAprep Spin Miniprep Kit. Half of the bacteria were transferred to 1.5 ml microtube and centrifuged in RT at 10000 rpm for 60 seconds. The supernatant was discarded and the previous step was repeated with the rest of the bacteria. Subsequently, the cellular pellet was resuspended in 250 µl of Buffer P1 (50mM Tris-HCl, 10mM EDTA, 100µg/ml RNase A). 250 µL of Buffer P2 (200mM NaOH, 1% SDS) was added and the mixture was vortexed. In the next step, 350 µl of Buffer N3 (composition confidential) was added, the solution was mixed by inverting the tube 6 times and left for 60 seconds for the precipitation to occur. The mixture was centrifuged at 13,000 rpm for 10 minutes.

800 µL of supernatant was applied onto the QIAprep 2.0 Spin Column, containing a silica membrane which binds DNA. The spin column was inserted in 1.5 ml microtube and centrifuged at 13,000 rpm for 60 seconds. The column was washed with 750 µl of Buffer PE (composition confidential) and centrifuged again at the same speed for 60 seconds. The eluant was discarded and the empty column was once again centrifuged for 60 seconds to ensure removal of any residual buffer. The column was transferred to clean 1.5 ml microtube, 50 µL of Buffer EB (10 mM Tris-HCl, pH 8.5) was applied directly onto the membrane, incubated for 60 seconds and centrifuged as in previous steps.

The concentration of DNA was measured using NanoDrop One/One Microvolume UV-Vis Spectrophotometer from Thermo Fisher Scientific.

5.2.3. Plasmid DNA bulk isolation using DNA-binding silica column

In order to yield a higher amount of plasmid and the possibility to filter any residual bacterial contaminants, a PureYield Plasmid Midiprep was done. One colony obtained during the previous transformation was transferred into 5 ml of LBA medium and incubated on a shaker overnight at 37 °C.

The next day, 3 ml of the mixture was transferred to 200 ml of LBA liquid medium in Erlenmeyer culture flasks and incubated overnight on a shaker at 37 °C. After the incubation, the mixture was transferred to 50 ml centrifuge tubes and the pellet was formed in a centrifuge at 5000 g for 10 minutes. The supernatant was discarded, and cells were resuspended in 3 ml of Cell Resuspension Solution (50mM Tris-HCl (pH 7.5), 10mM EDTA (pH 8.0), 100µg/ml RNase A). The Cell Lysis Solution (0.2M NaOH, 1% SDS) was added in the same amount and the tubes were mixed by inverting 3-5 times. The tubes were incubated at room temperature for 3 minutes. Neutralization Solution (4.09M guanidine hydrochloride (pH 4.2), 759mM potassium acetate, 2.12M glacial acetic acid) was added in the amount of 5 ml, the tubes were mixed 10 times by inverting and incubated for 5 minutes at room temperature for the precipitate to form.

The lysate was poured to the Clearing Column that was placed in a clean 50 ml centrifuge tube and let sit for 2 minutes. The tube was centrifuged uncapped at 3000 g for 5 minutes using the swinging-bucket rotor. The filtrate was poured to the Binding Column, that was placed in a clean 50 ml centrifuge tube. The tube was centrifuged at 3000 g for 5 minutes. On the column,

20 ml of Wash Solution (162.8mM potassium acetate, 22.6mM Tris-HCl (pH 7.5), 0.109mM EDTA (pH 8.0)) was added and centrifuged for 5 minutes at 3000 g. The supernatant was discarded and column centrifuged for an additional 10 minutes do clean the binding membrane from any residual ethanol. The column was transferred to clean 50 ml centrifuge tube and 600 µl of nuclease-free water was added on top of the membrane drop-wise. The column was centrifuged for the last time at 2000 g for 5 minutes. The filtrate was transferred to 1,5 ml microtube.

The concentration of DNA was measured as mentioned in 5.2.2.

5.3. Preparation of HeLa cells for transfection

An important tool in any molecular biology research is immortalized cell lines, a population of cells from a multicellular organism that has evaded normal cellular senescence and instead keep undergoing division. This is the reason why they can be cultured in the *in vitro* conditions for prolonged periods of time. For this reason, they are used as a model for a more complex biological system.

For the purpose of this experiments immortal cell line, HeLa was used. HeLa cells are cervical cancer cells isolated from deceased American cancer patient Henrietta Lacks. They are the oldest used immortal cell line. The cell line grows adherently as a monolayer.

5.3.1. Cell thawing

Before the experiment, the cell lines were thawed. The vials were taken out of the liquid nitrogen and put in a heating bath with aluminium beads heated to 37 °C for one minute. Immediate resuspension of the cells in Dulbecco's modified medium (DMEM) with 10 % foetal bovine serum (FBS) is crucial to ensure high viability of the cells. The cells are frozen in 10% dimethyl sulfoxide (DMSO) which is toxic for the cells and the DMEM is used to dilute DMSO, thus prevent its toxic effects on the cells. Completely thawed cells in DMEM were transferred into 10 cm cell culture dish, the media with cells was spread on it with eight-shaped motion and kept in cell culture incubator at 37 °C, 5% CO2.

Next day, the cells were inspected under a light microscope to check their growth progress and viability. The media was aspired with a pipette and replaced with fresh low glucose DMEM with 10 % FBS, 1 % glutamine and 1 % antimycotic/antibiotic.

5.3.2. Cell subculturing

HeLa is an adherent type of cell line and stops proliferation after reach the confluency. Because of this, it needs to be regularly passaged before reaching complete confluency to prevent unwanted differentiation and induction of senescence phenotype. We decided to use this cell line because they are easy to transfect. It will serve as a model for subsequent research.

The process of subculturing of the cell line has to be done in the aseptic environment. An old medium was aspirated and cells were carefully washed with sterile phosphate-buffered saline (PBS). To detach the cells from the surface 2 ml of Trypsin (25 mM) was applied and incubated for a few minutes at 37 °C. Trypsin was inactivated by addition of 5 ml of fresh full DMEM. The plate was washed several times with the light flow of medium from a serological pipette to secure complete cell detachment. Cells were removed from the culturing plate and place into a 10 ml centrifuge tube. The medium was diluted as needed and put into culture flask for further growth of the cell line.

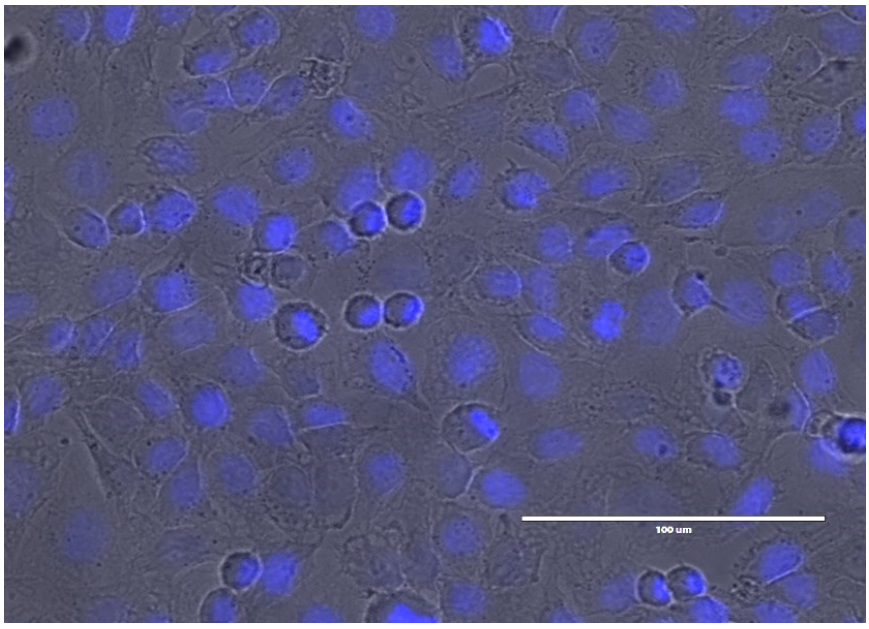

Figure 6: Fluorescence image of HeLa cells with a visualised nucleus (blue). Magnification 40x.

5.3.3. Cell seeding

One day before transfection, cells were seeded on a glass coverslip inserted into 24-well plate. To ensure the same condition for further cell transfection the same number of cells in each experiment (i.e. well) is needed and therefore the cells must be counted and seeded at the same concentration.

Firstly, the medium was aspirated from the cell culture dish/flask and cells were washed with sterile PBS. To detach the adherent cells from the surface, 2 ml of 0,25% Trypsin was used and the flask was incubated for 2 minutes at 37 °C in the CO2 incubator. Next, 5 ml of DMEM was added to deactivate Trypsin and resuspend cells. 10 µl Trypan Blue was added to 10 µl of the cell suspension and mixed. 10 µl of this suspension was pipetted onto the Neubauer counting chamber and counted as depicted in Figure 7 in five out of all nine squares. The average of the counted cells was taken and diluted with the volume needed to achieve the number of cells. Cells were seeded at the density $5*10^4$/ml in 24-well and incubated at 37 °C in a CO2 incubator.

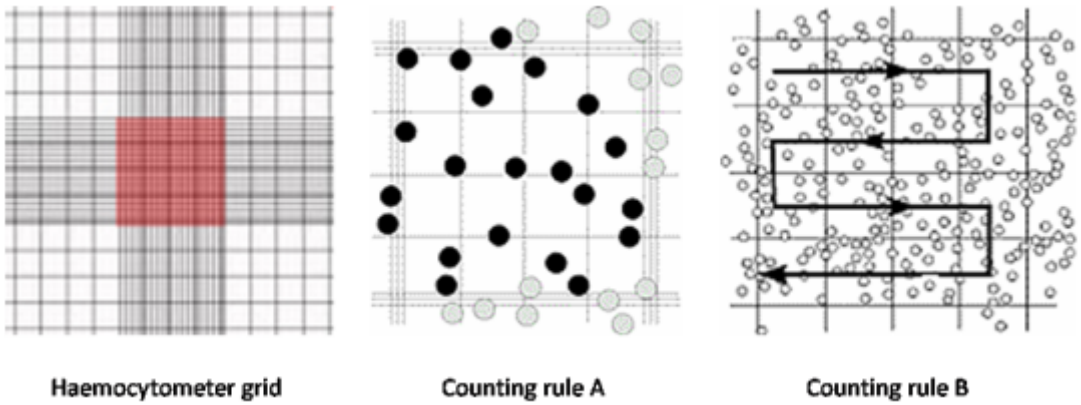

Figure 7: Neubauer chamber counting plate (left), with cell counting rules. (B110 Editor 2010)

5.4. Transfection of HeLa cells

Transfection is a molecular biology method of introduction of nucleic acid into eukaryotic cells. It is used for the study of gene function and regulation and protein function. The introduced genetic materials can exist in cells either stably or transiently depending on the nature of the genetic material and the method of transfection. Stable transfection is characterised by an integration of the foreign DNA into the host genome and expressed constantly. In the case of transient transfection, foreign DNA is not integrated into the genome and the expression can be

halted by environmental factors or cell division. Both stable and transient gene expression has its benefits and disadvantages so the choice depends on the objective of the experiment.

In our experiments, we opted for transient transfection using chemical methods, using commercially available PolyJet DNA *In Vitro* Transfection Reagent. PolyJet is a cationic polymer that forms complexes between the reagent and pDNA. The complexes are subsequently transported into the cells via endocytosis. PolyJet Reagent is not toxic to the mammalian cells due to the rapid and complete degradation of the polymer. The manufacturer SignaGen Laboratories states that the efficiency of transfection is 88% in the case of HeLa cells. (SignaGen Laboratories 2020)

5.4.1. Transient transfection of HeLa cells for localization of FUBP3

Plasmid vector containing FUBP3 cDNA (pCMV-FALG-FUBP3) used in our experiments was previously prepared at the Faculty of Pharmacy University of Ljubljana. For the backbone of the plasmid, a commercially available pCMV-FLAG plasmid was chosen. At the N-terminus of the protein, the FLAG tag is added and fusion protein which can be detected with anti-FLAG antibody. The plasmid also carries the gene for beta-lactamase, hence it gives the bacterial cell resistance against ampicillin which is used for selection of bacterial colonies with the expression of the desired protein.

For transfection, HeLa cells attached on glass coverslip inserted in the 24-well plate were used. 500 ng of plasmid was added to 25 µl of serum-free DMEM for each well. In parallel, 1.5 µl of PolyJet was added to 25 µl of serum-free DMEM per transfected well. Both solutions were mixed thoroughly by vortexing. PolyJet solution was added to the microtube with pDNA and the prepared mixture was mixed by aspirating a few times with pipette. The microtube was left at room temperature (RT) for approximately 15 minutes for the pDNA-PolyJet complexes to form. The pDNA-PolyJet solution was added drop-wise to each well with cells. The plate was swirled gently so everything is properly mixed. The plates were put in 37 °C CO2 incubator for 24 hours.

5.4.2. Transient transfection of HeLa cells for silencing of FUBP3 expression

Gene silencing is a molecular biology technique which aims to interfere with gene expression of a specific gene with a complementary sequence to the used „silencing“ nucleic acid. The

silencing can occur at the level of transcription as well as at the level of translation. The main methods of gene silencing are using antisense oligodeoxynucleotides, ribozymes and DNA enzymes and by RNA interference. The gene silencing reduces the expression of a gene that makes it distinct from gene knock-out methods erasing the gene from the organism's genome and thus halting the expression completely.

For our experiments, we have chosen the RNA interference method. This method is characterized by selective inactivation of the studied protein's mRNA by double-stranded RNA. More precisely we have opted for the use of short hairpin RNA (shRNA), which contains a loop structure that is later processed to short interfering RNA (siRNA). The siRNA binds to a complementary part of mRNA and ultimately leads to mRNA degradation.

The shRNA was introduced into the cells via transient transfection using a chemical method with PolyJet DNA *In Vitro* Transfection Reagent kit. The FUBP3 shRNA Plasmid (h) (sc-106747-SH; Santa Cruz Biotechnology) is a pool of 3 target-specific lentiviral vector plasmids each encoding 19-25 nucleotides (plus hairpin) shRNAs. The plasmid also contains the puromycin resistance gene for the selection of cells stably expressing shRNA. As a negative control, a Control shRNA Plasmid-A (sc-108060, Santa Cruz Biotechnology) was used.

The transfection itself was done in the same manner as the transfection of the pCMV-FLAG-FUBP3 plasmid mentioned in section 5.4.1.

5.5. Visualisation of investigated proteins by immunofluorescence microscopy

Immunofluorescence is a technique that uses the specificity of antibodies to their antigen to bind particular cell structures. It is based on using a fluorescent probe that is further visualized by absorbing light of specific wavelength and emitting light of different (longer) wavelength, that is detected. Fluorescing probe, the fluorophore can be conjugated either to the primary or the secondary antibody. Both methods have advantages and disadvantages and it is up to the researcher to choose the right one for their experiment. We have chosen an indirect immunofluorescence for our experiments.

5.5.1. Immunostaining of investigated proteins

For immunostaining of the investigated proteins, the following protocol was employed. Firstly, the medium was aspirated from the well and cells were washed with PBS. Cells were fixed to glass in each well by adding 500 µl of 4% paraformaldehyde in PBS and left to incubate at RT for 15 minutes. Then, the cells were washed with PBS three times for 5 minutes. Next step was permeabilization with 300 µl of 1% bovine serum albumin (BSA) and 0.2% Tween in PBS and incubated at RT for 5 minutes. The following step was to wash the cells again with PBS this time twice each washing being 5 minutes. To prevent unspecific specific binding of antibodies to non-target cell structures 300 µl of 3% skim milk was added to each well and incubated at RT for 30 minutes. The cells were washed with PBS twice for 5 minutes. In the next step, 200 µl of primary antibody (pAb) with the desired dilution was added to each well and left to incubate at room temperature for 2 hours. The solution of pAb was aspirated with pipette and cells were washed with PBS twice for 5 minutes. 200 µl of sAb in the desired dilution was added to each well, left for 45 minutes at room temperature and covered with foil. In the end, the solution of the secondary antibody was aspirated with pipette and cells were washed with PBS twice for 5 minutes.

Altogether, four different immunostaining experiments were performed. The used combinations of pAb and sAb, as well as their concentrations for each experiment, are described in the following sections.

5.5.1.1. Localisation of FUBP3

The localisation was examined with either endogenous or overexpressed FUBP3. Following primary antibody was used: mouse anti-FLAG antibody (Sigma Aldrich; F3165) in dilution 1:1000, and mouse anti-FUBP3 (Santa Cruz Biotechnology; sc-398466) in dilution 1:200. As a secondary one, donkey anti-mouse IgG (H+L) antibody conjugated with Alexa Fluor (AF) 555 (Thermo Fisher Scientific; A31570) in dilution 1:1000 was used. This antibody emits orange light after exposure to light with 555nm wavelength. All of the antibodies were diluted to the desired dilution in 3% BSA in PBS.

Investigated protein	Primary antibody	Secondary antibody
Overexpressed FUBP3	Anti-FLAG, 1:1000	Anti-ms IgG AF 555, 1:1000
Overexpressed FUBP3	Anti-FUBP3, 1:200	
Endogenous FUBP3	Anti-FLAG, 1:1000	
Endogenous FUBP3	Anti-FUBP3, 1:200	
Endogenous FUBP3	X	

Table 1: Primary and secondary antibodies used for localization of FUBP3 in HeLa cells. AF - Alexa Fluor

5.5.1.2. Optimization of Golgi apparatus immunostaining

Six different concentrations of antibody rabbit anti-GM130 (Sigma Aldrich; G7295) were used for optimization as depicted in Table 2. As secondary antibody, goat anti-rabbit IgG antibody conjugated with Alexa Fluor 488 (Thermo Fisher Scientific; A11008) in dilution 1:1000 was chosen. This antibody emits green light after exposure to light with 496 nm wavelength. All of the antibodies were diluted to the desired dilution in 3% BSA in PBS.

Exp.	Primary antibodies	Secondary antibodies
1	Anti-GM130, 1:200	Anti-rb IgG AF 488, 1:1000
2	Anti-GM130, 1:500	
3	Anti-GM130, 1:1000	
4	Anti-GM130, 1:1500	
5	Anti-GM130, 1:2000	
6	Anti-GM130, 1:2500	
7	X	

Table 2: Primary and secondary antibodies used for the optimization of GA immunostaining in HeLa cells. AF – Alexa Fluor

5.5.1.3. Co-localization of FUBP3 and Golgi apparatus

For localization of FUBP3 in endogenous and overexpressed form, the same antibodies as mentioned in section A) were used. For visualization of Golgi apparatus, rabbit anti-GM130 (Sigma Aldrich; G7295) in dilution 1:500. Secondary antibodies used were: for localisation of FUBP3 as mentioned in section 5.5.1.1.; for localisation of GM-130 as mentioned in section 5.5.1.2.

Investigated protein	Primary antibodies	Secondary antibodies
Overexpressed FUBP3	Anti-FLAG, 1:1000 Anti-GM130, 1:500	Anti-ms IgG AF-555, 1:1000 Anti-rb IgG AF-488, 1:1000
Overexpressed FUBP3		
Endogenous FUBP3		
Endogenous FUBP3		
Endogenous FUBP3	X	

Table 3: **Primary and secondary antibodies used for co-localization of FUBP3 and GA in HeLa cells.** AF – Alexa Fluor

5.5.1.4.Confirmation of FUBP3 silencing

For confirmation of the efficacy of *FUBP3* gene silencing in HeLa cells, we used immunofluorescent detection of the target protein. Experiments were performed in cells with endogenous production of FUBP3 or overexpressed production of FUBP3. In parallel to shRNA silenced FUBP3, also experiments without shRNA were performed. Antibodies used for visualisation of FUBP3 is mentioned in section 5.5.1.1. All of the antibodies were diluted to the desired dilution in 3% BSA.

Exp.	Transfection	Protein examined	Primary antibodies	Secondary antibodies
1	X	Endogenous FUBP3	Anti-FUBP3 1:200	Anti-ms IgG AF-555, 1:1000
2	shRNA FUBP3	Endogenous FUBP3 + shRNA		
3	shRNA FUBP3, pCMV-FLAG-FUBP3	FUBP3		
4	pCMV-FLAG-FUBP3	FUBP3		
5	Control shRNA Plasmid-A	FUBP3		

Table 4: Primary and secondary antibodies used for silencing of FUBP3 expression in HeLa cells. AF – Alexa Fluor.

5.5.2. Immunofluorescence microscopy

After immunostaining, the microscopy glasses were prepared and on each, a drop of ProLong Gold Antifade Mountant with DAPI was added. The coverslips were taken out of the wells and carefully placed on the drop of the mounting reagent in a way that the side with cells was facing the drop of mounting reagent. The coverslip was slightly pressed to ensure no air bubbles are underneath it and the slips were secured with colourless nail polish. The microscope glasses were left overnight in a dark box in the fridge for the mountant to properly dry. On the next day, the coverslips were sealed with colour-less nail polish to prevent further drying of the mountant.

The images were acquired using the EVOS® FL Cell Imaging System from Thermo Fisher Scientific. Usually, five sets of images (each image recording different fluorescent channel) from each coverslip were generated. The possible magnification was from 4x to 40x.

6. Results

6.1. The localisation of FUBP3 in HeLa cells

First, we sought to set a protocol for visualisation of FUBP3 in HeLa cells using immunofluorescence. Since proteins are investigated while being overexpressed as well as the natural level of expression, we have to optimise immunofluorescence protocols, especially antibody concentrations.

The pCMV-FLAG-FUBP3 plasmid was introduced to HeLa cells. The efficiency of transfection was checked by the green fluorescence of the GFP protein successfully incorporated into the host genome (Fig. 8). During transient transfection, cell intakes the construct of transfection reagent via endocytosis. The reagent is then degraded, and plasmids are translocated to the nucleus where the cDNA is transcribed. Therefore, the transcribed proteins of the exogenous origin have the FLAG-tag that allows easy detection of the protein by anti-FLAG antibody and distinguished from endogenously transcribed protein.

For detection of overexpressed FUBP3, we have chosen the concentration of anti-FLAG antibody (1:1000). We have detected the signal both in cytosol and nucleus. The signal was not observed in all of the cells, but only in the transfected ones. (Fig. 9) The same was observed while using the anti-FUBP3 antibody (1:200) in the cells with overexpressed FUBP3 (Fig. 10)

Endogenous FUBP3 was detected with anti-FUBP3 antibody in concentration 1:200. A weak signal could be seen in the cells mainly around nuclei with only a few cells with a signal in nuclei as well (Fig. 11)

The specificity of anti-FLAG antibodies was tested by staining untransfected cells. No signal comparable to the other experiments was observed. (Fig. 12) The specificity of secondary antibody (sAb) was investigated by staining of cells only with sAb in concentration 1:1000, without previous incubated with pAb. No visible signal was observed here as well. (Fig. 13)

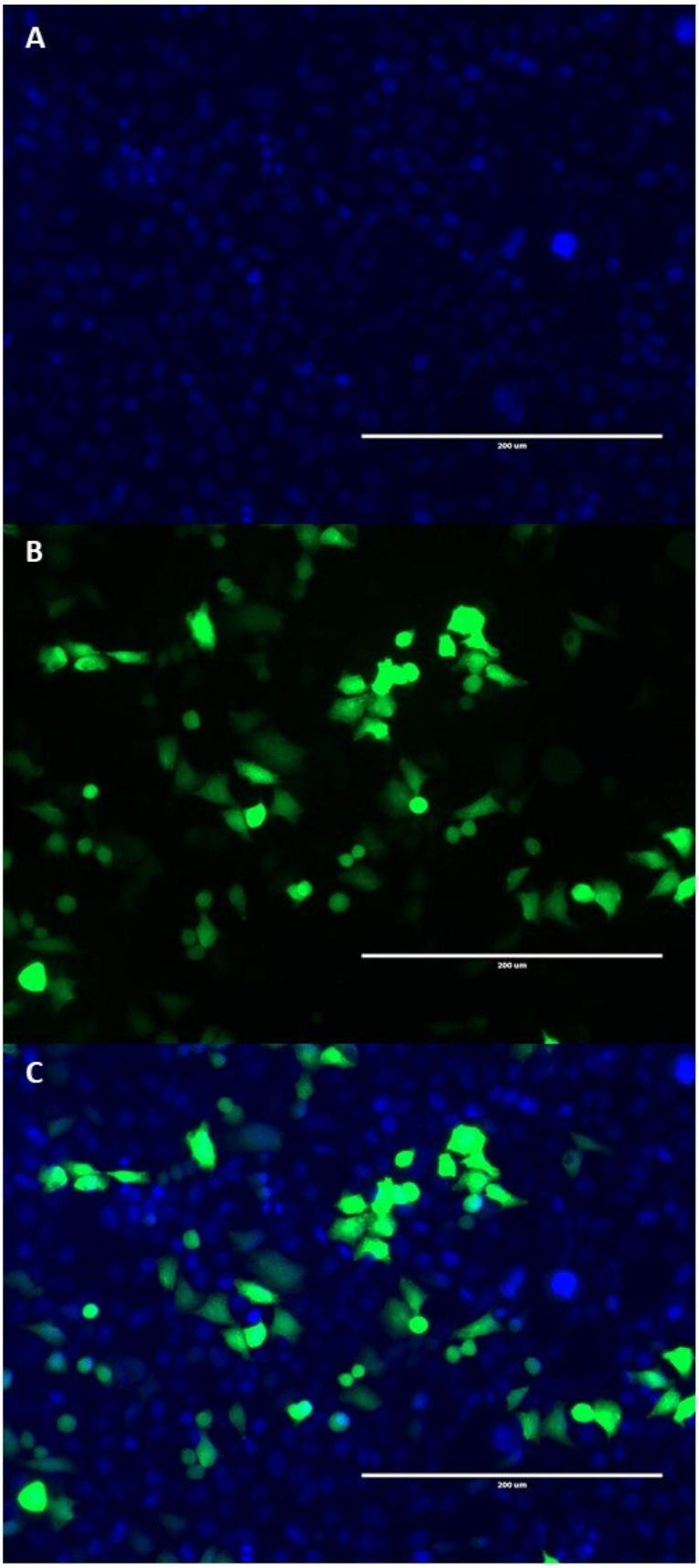

Figure 8: Control of cell transfection with GFP (magnification 20x); **A**) nuclei stained with DAPI (blue), **B**) visualised GFP (green), **C**) images A and B merged.

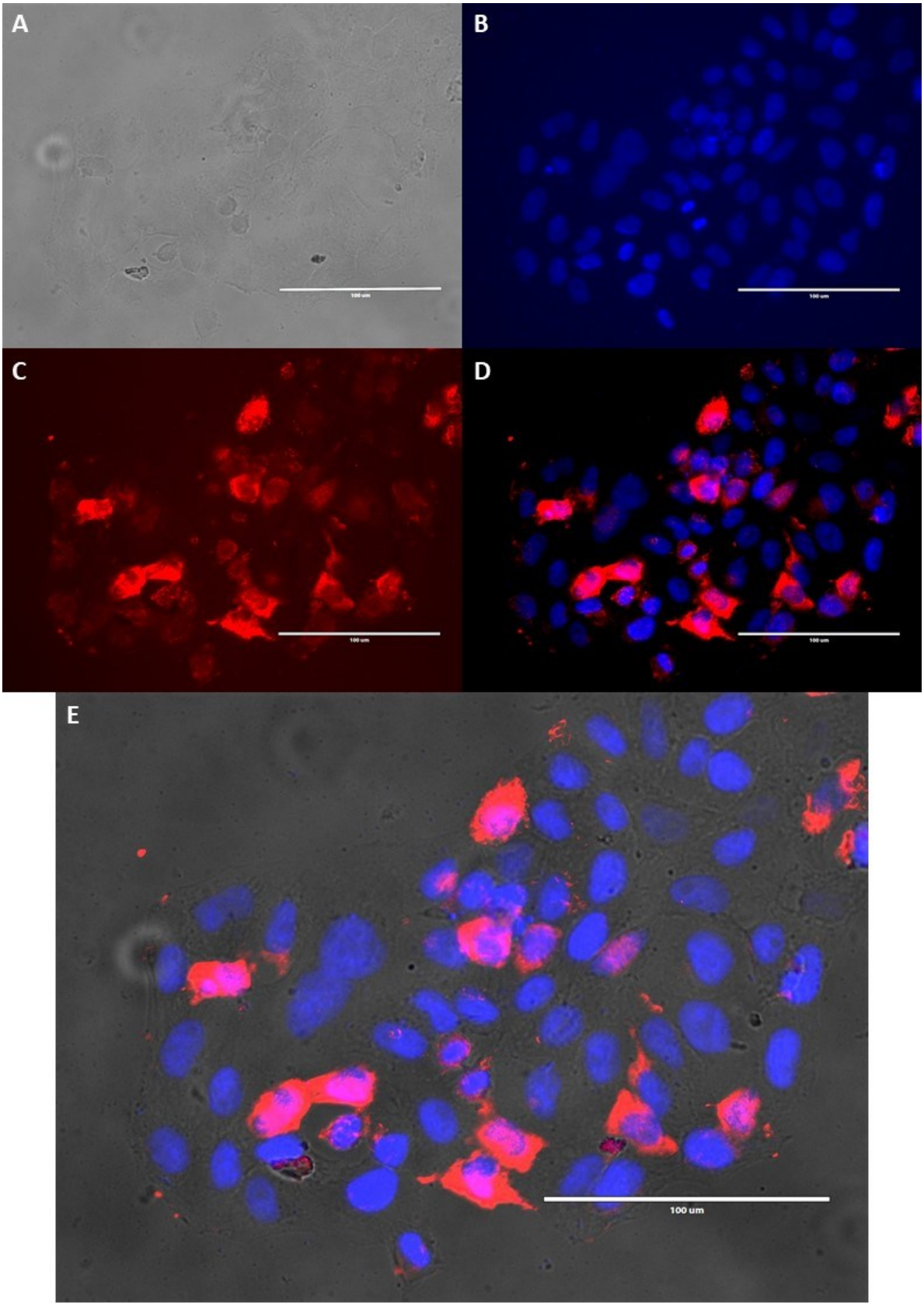

Figure 9: Immunofluorescence of overexpressed FUBP3, anti-FLAG antibody (1:1000), (magnification 40x); **A**) cells in bright-field, **B**) nuclei stained with DAPI (blue), **C**) visualised FUBP3 (red), **D**) visualised nuclei and FUBP3, **E**) images A-D merged.

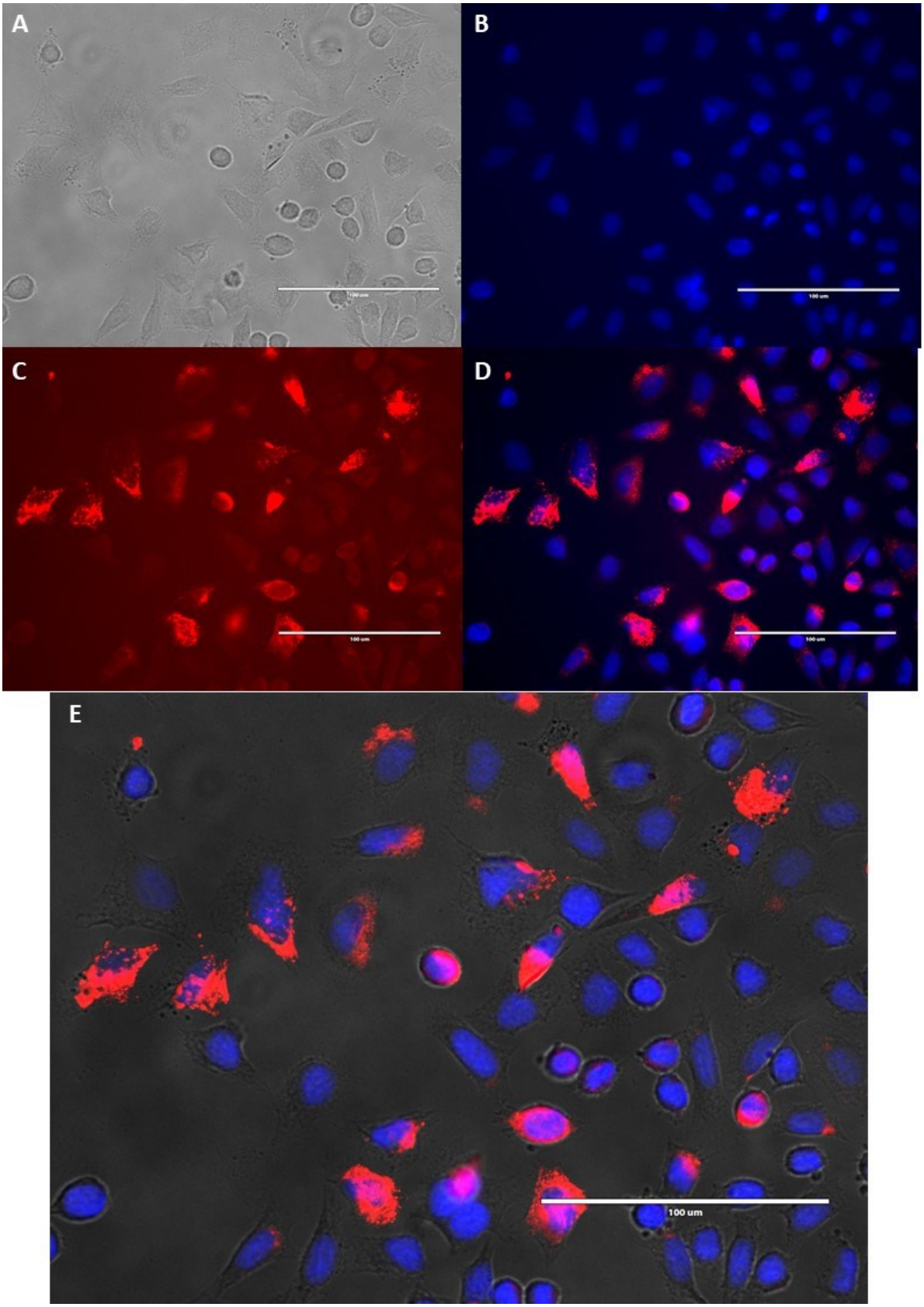

Figure 10: Immunofluorescence of overexpressed FUBP3, anti-FUBP3 antibody (1:200), (magnification 40x); **A**) cells in bright-field, **B**) nuclei stained with DAPI (blue), **C**) visualised FUBP3 (red), **D**) visualised nuclei and FUBP3, **E**) images A-D merged.

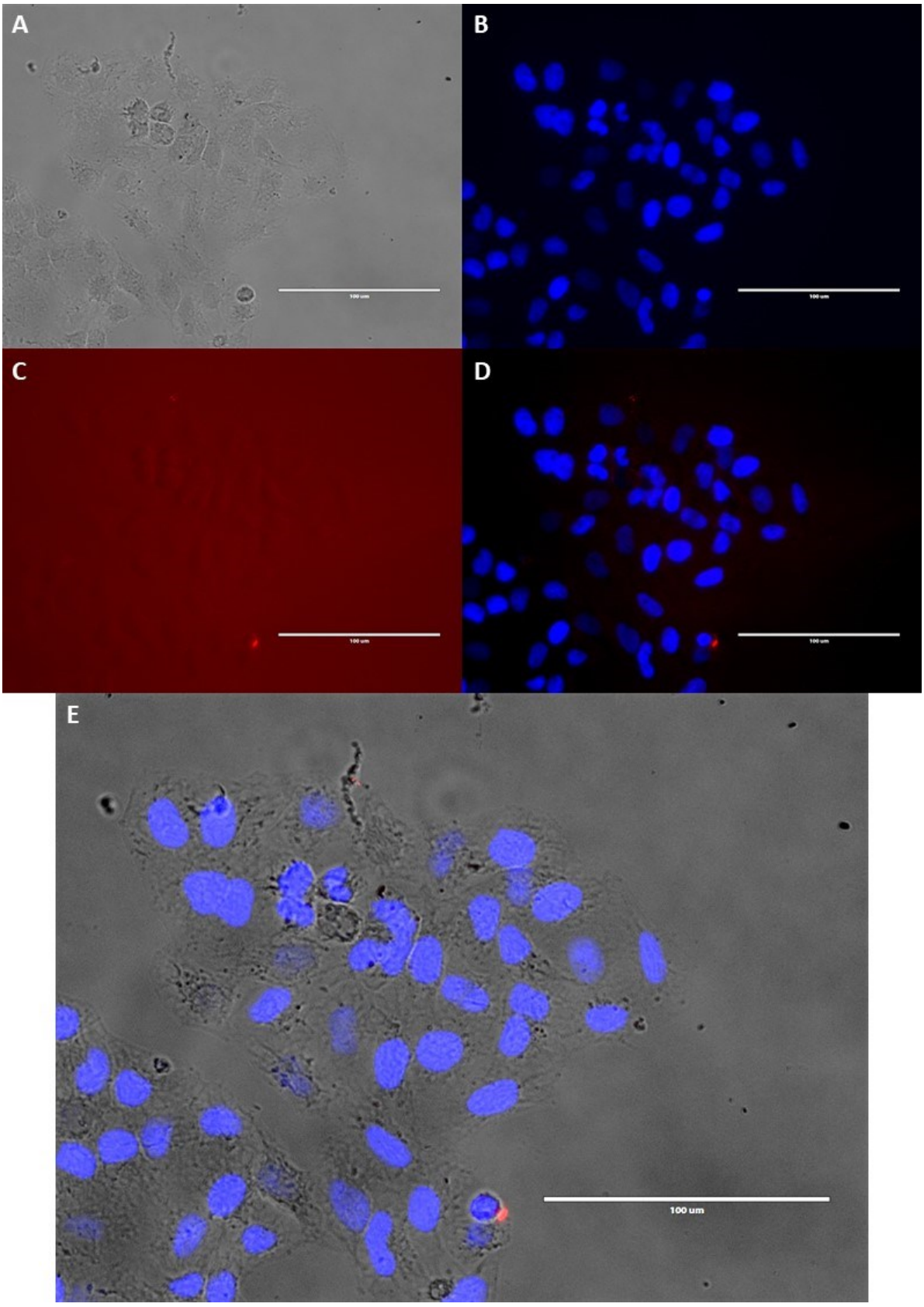

Figure 11: Immunofluorescence of endogenous FUBP3, anti-FLAG antibody (1:1000), (magnification 40x); **A**) cells in bright-field, **B**) nuclei stained with DAPI (blue), **C**) visualised FUBP3 (red), **D**) visualised nuclei and FUBP3, **E**) images A-D merged.

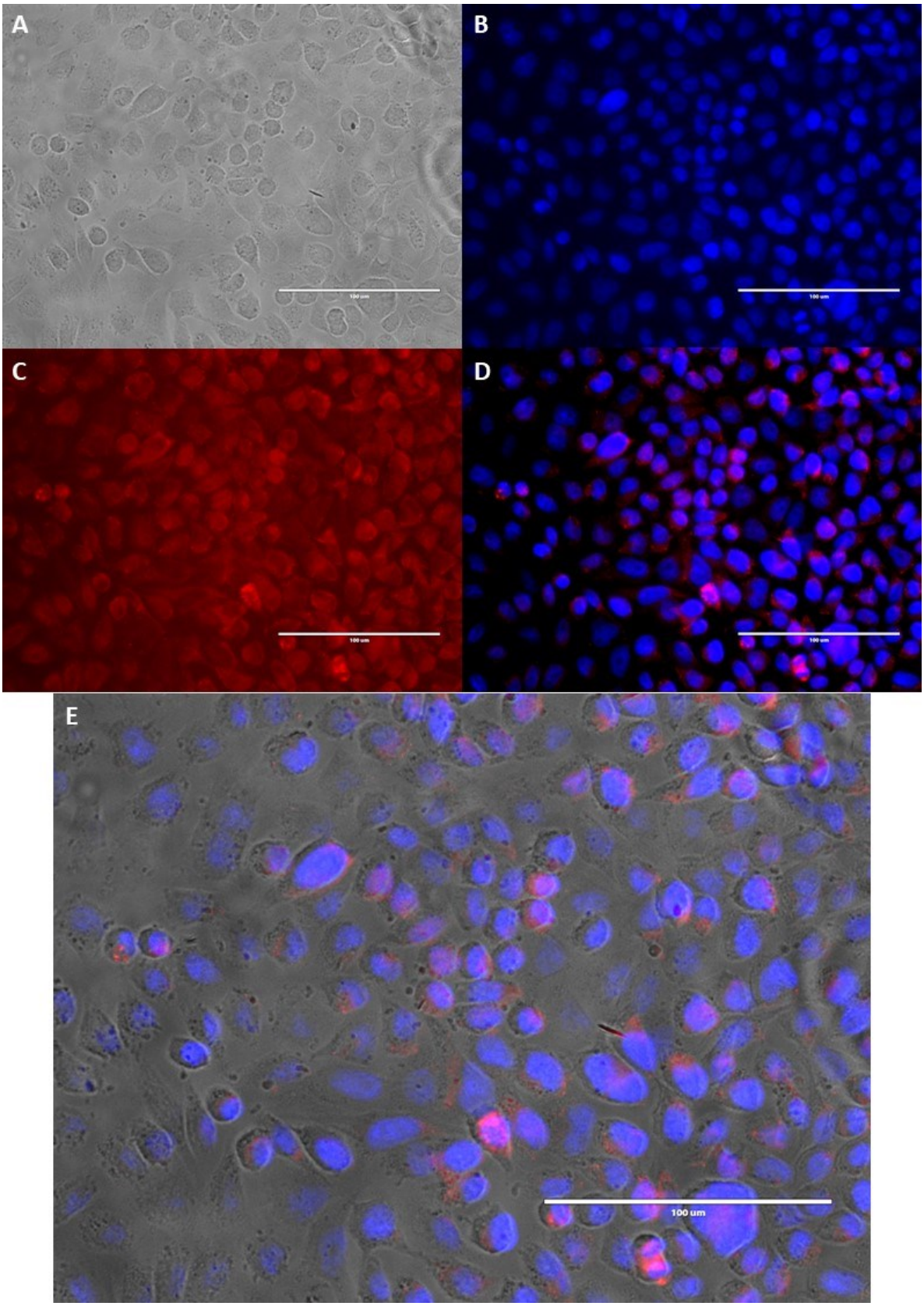

Figure 12: Immunofluorescence of endogenous FUBP3, anti-FUBP3 antibody (1:200), (magnification 40x); **A**) cells in bright-field, **B**) nuclei stained with DAPI (blue), **C**) visualised FUBP3 (red), **D**) visualised nuclei and FUBP3, **E**) images A-D merged.

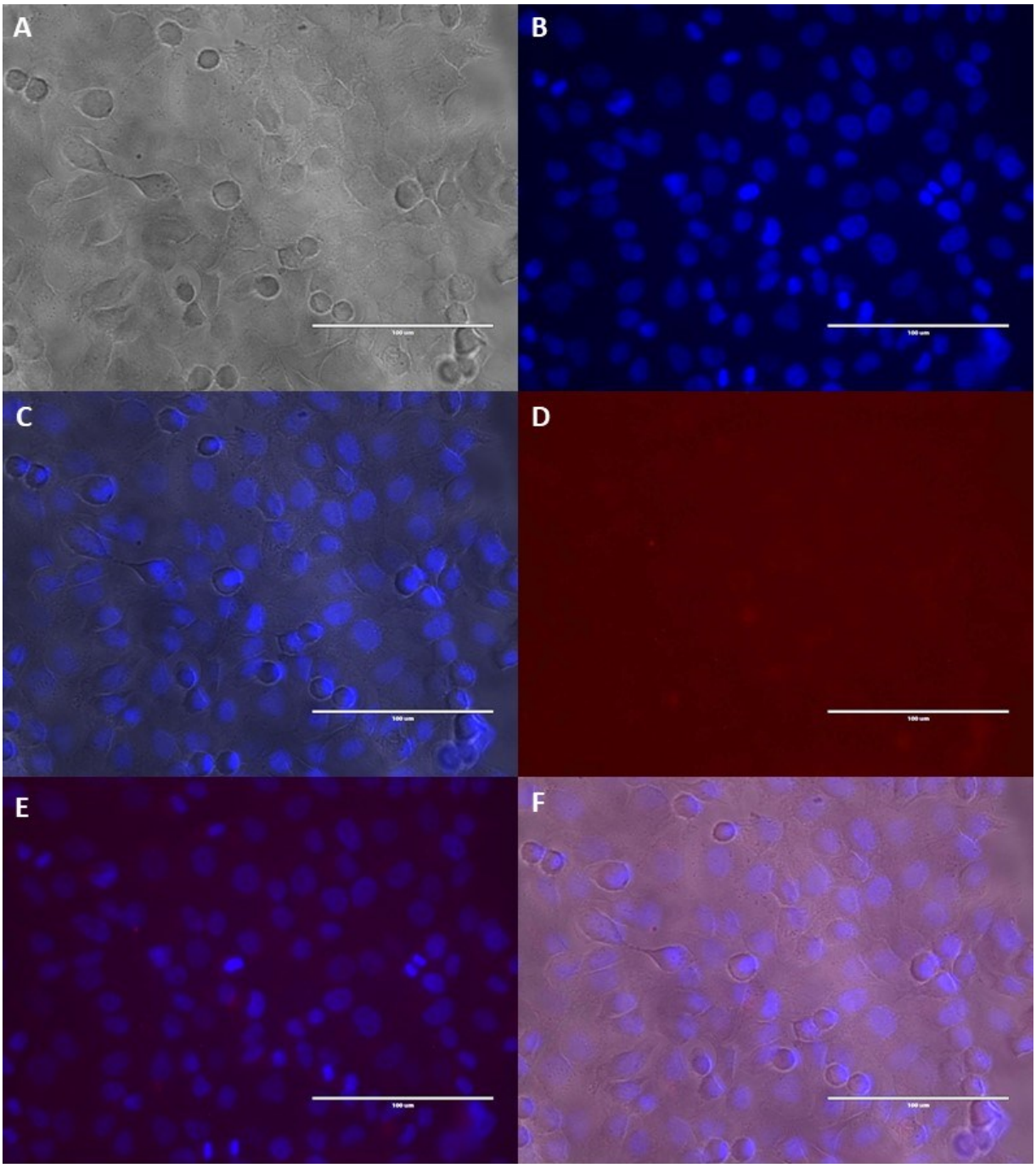

Figure 13: Control for specific binding of secondary antibodies, anti-ms Alexa Fluor 555 (1:1000) (magnification 40x); **A**) cells in bright-field, **B**) nuclei stained with DAPI (blue), **C**) visualised nuclei and bright-field, **D**) visualised anti-ms IgG AF 555 (red), **E**) visualised nuclei and FUBP3, **F**) images A-E merged.

6.2. Optimization immunostaining for of Golgi apparatus in HeLa cells

To further investigate whether at least part of cytosolic FUBP3 is located in the Golgi apparatus (GA) in HeLa cells, the method of co-immunostaining was chosen. For detection of GA a specific marker, peripheral cytoplasmic Golgi Matrix Protein of 130 kDa (GM130) was used. The dilution of anti-GM130 antibody recommended by manufacturer was 1:2500; unfortunately, pilot experiments showed any results with this dilution. Therefore, we had to optimize pAb dilution before the co-localization of FUBP3 and Golgi apparatus in the HeLa cells was done. Dilutions of the anti-GM130 antibody for optimization were in a range from 1:200 to 1:2500.

First three, 1:200, 1:500 and 1:1000 dilutions proved to be promising in visualising Golgi apparatus. The signal from the 1:200 dilution was too strong for use in co-localization experiments. On the other side, the signal from the dilution 1:1000 was still visible, but it was too week for use in our experiment. Dilutions of 1:1500 and higher showed too little signal to be reliably used to visualise Golgi apparatus. Thus, the dilution of pAb 1:500 was chosen as the best one since it provided the most suitable intensity of the signal.

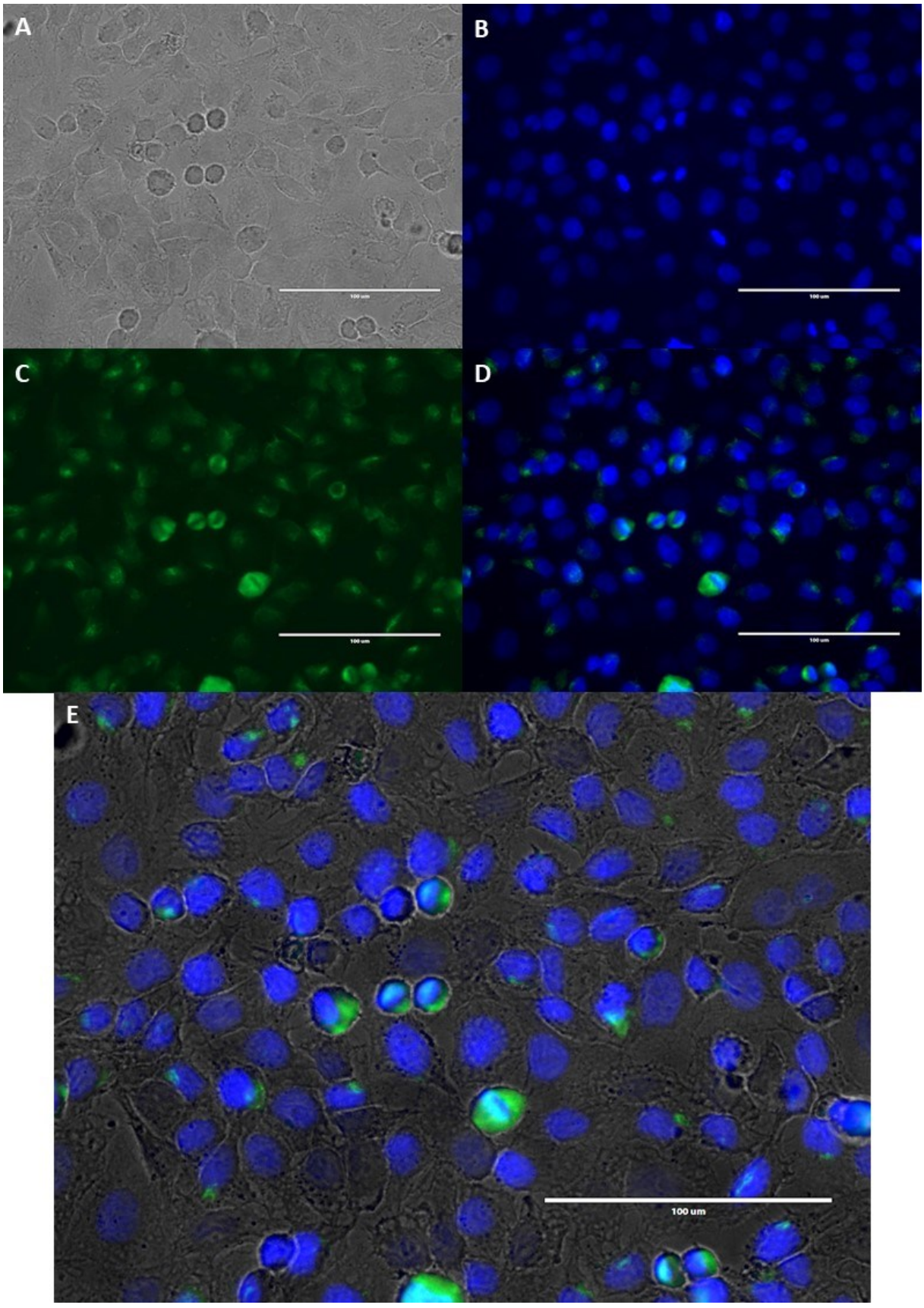

Figure 14: Optimization of GM130 visualisation, anti-GM130 1:200 (magnification 40x); **A**) cells in bright-field, **B**) nuclei stained with DAPI (blue), **C**) visualised GM130 (green), **D**) visualised nuclei and GM130, **E**) images A-D merged.

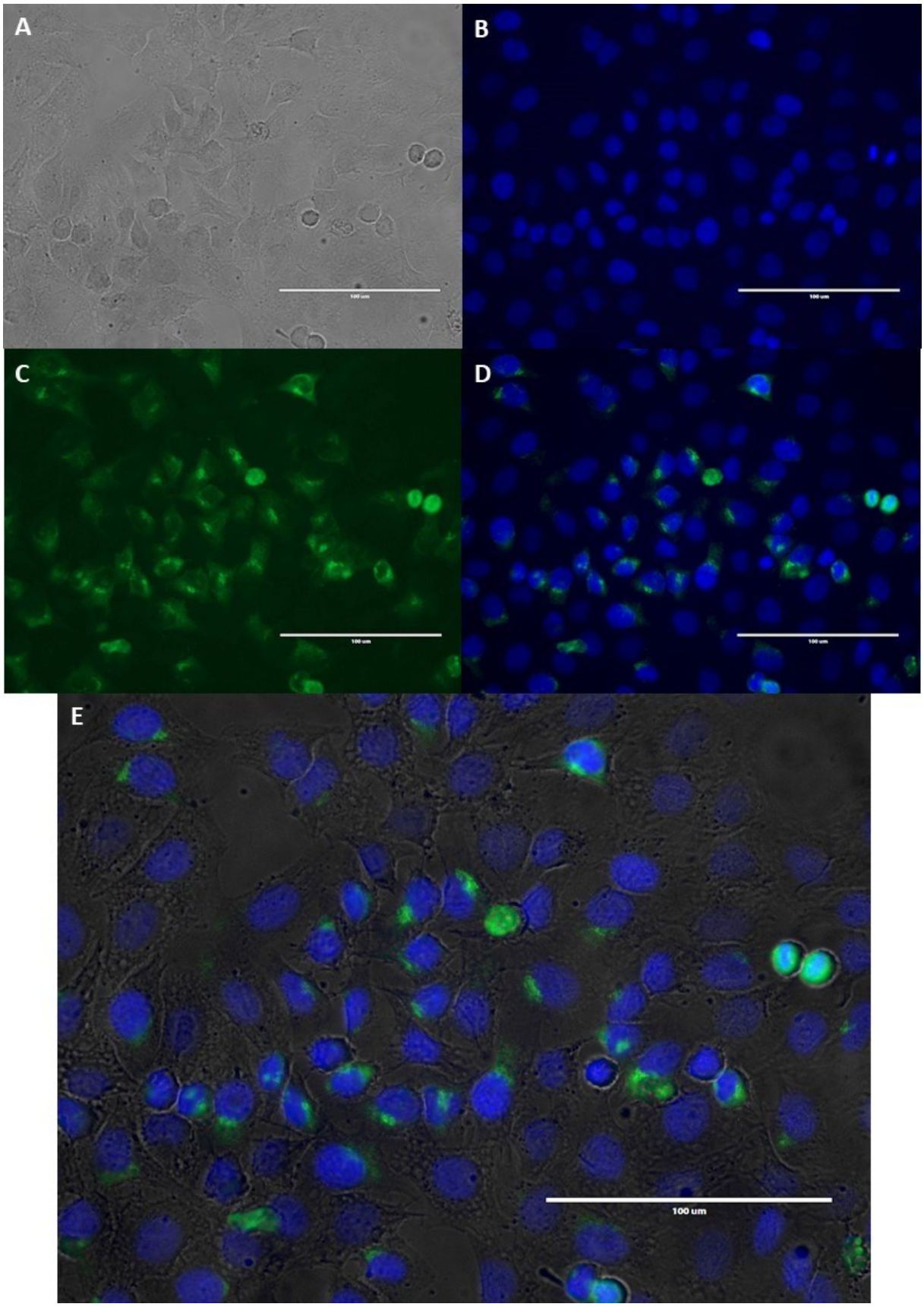

Figure 15: Optimization of GM130 visualisation, anti-GM130 1:500 (magnification 40x); **A**) cells in bright-field, **B**) nuclei stained with DAPI (blue), **C**) visualised GM130 (green), **D**) visualised nuclei and GM130, **E**) images A-D merged.

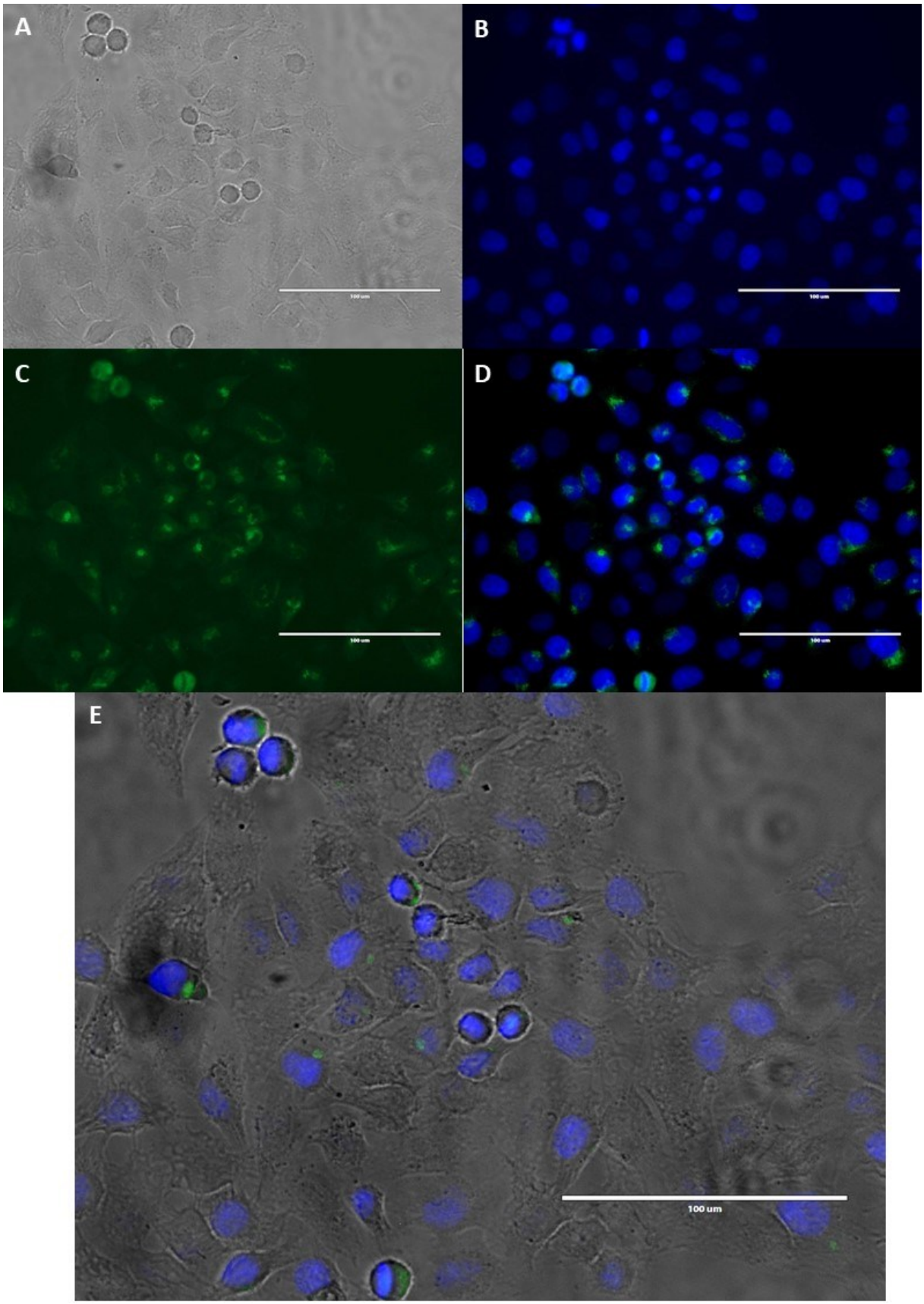

Figure 16: Optimization of GM130 visualisation, anti-GM130 1:1000 (magnification 40x); **A**) cells in bright-field, **B**) nuclei stained with DAPI (blue), **C**) visualised GM130 (green), **D**) visualised nuclei and GM130, **E**) images A-D merged.

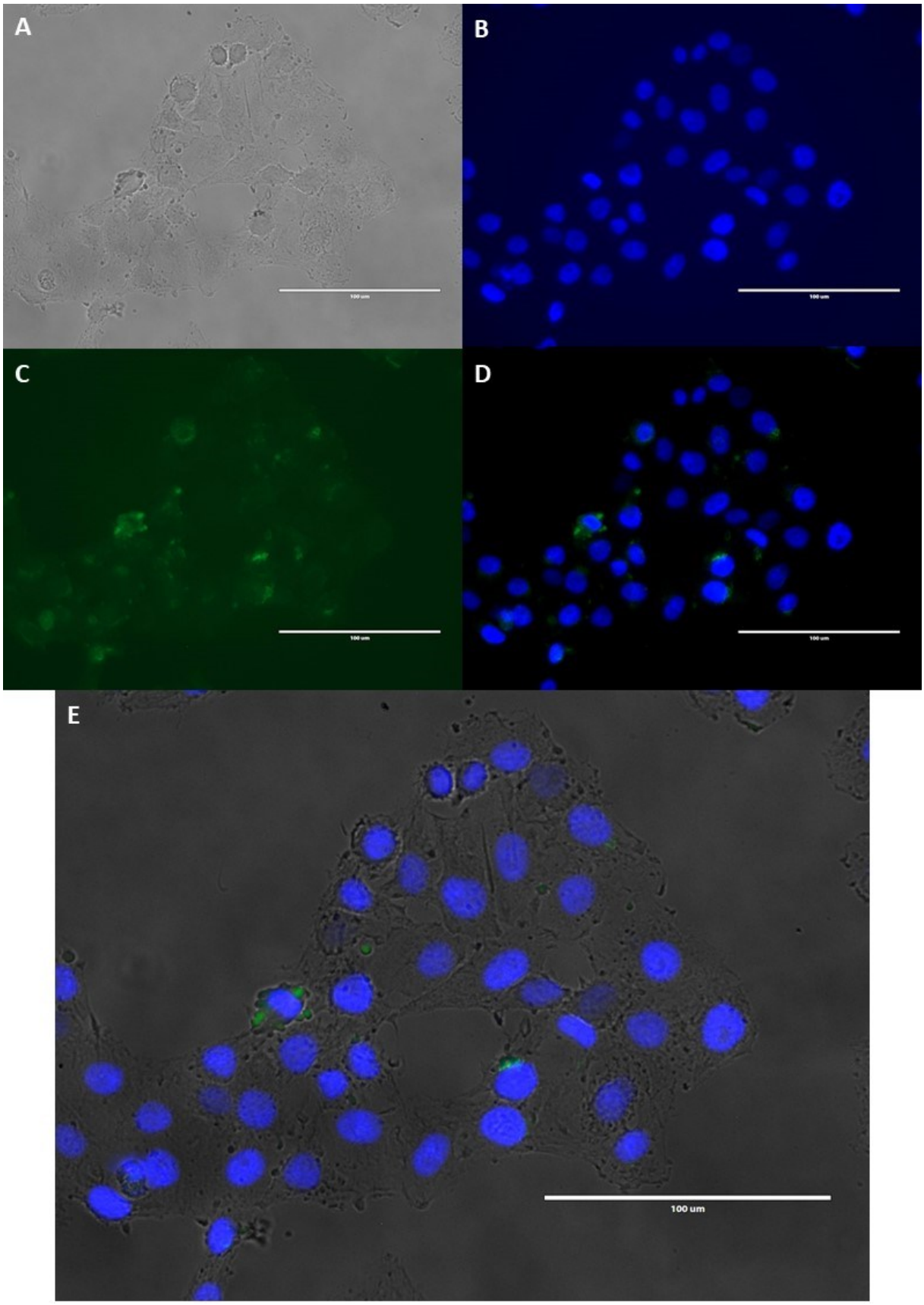

Figure 17: Optimization of GM130 visualisation, anti-GM130 1:1500 (magnification 40x); **A**) cells in bright-field, **B**) nuclei stained with DAPI (blue), **C**) visualised GM130 (green), **D**) visualised nuclei and GM130, **E**) images A-D merged.

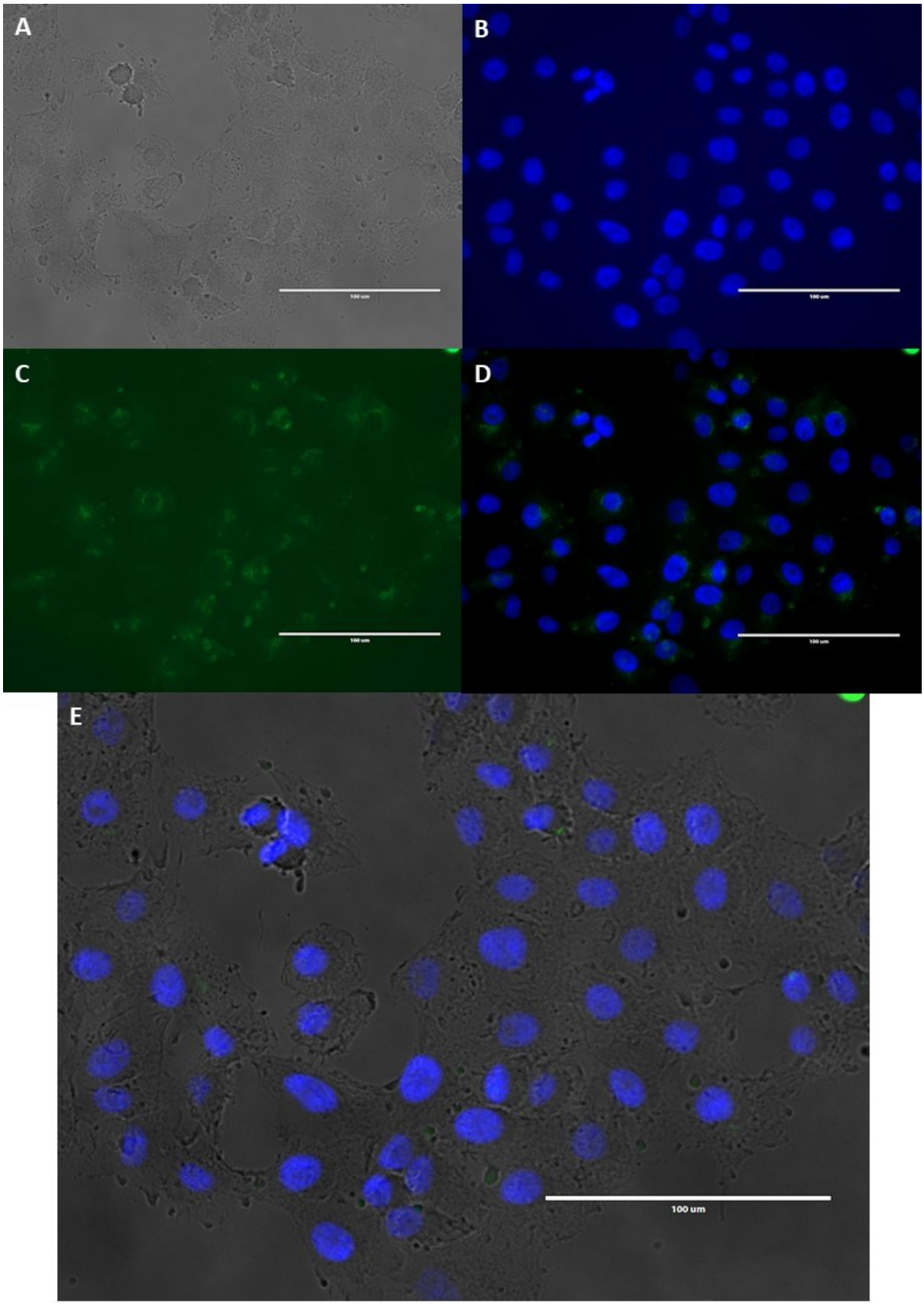

Figure 18: Optimization of GM130 visualisation, anti-GM130 1:2000 (magnification 40x); **A**) cells in bright-field, **B**) nuclei stained with DAPI (blue), **C**) visualised GM130 (green), **D**) visualised nuclei and GM130, **E**) images A-D merged.

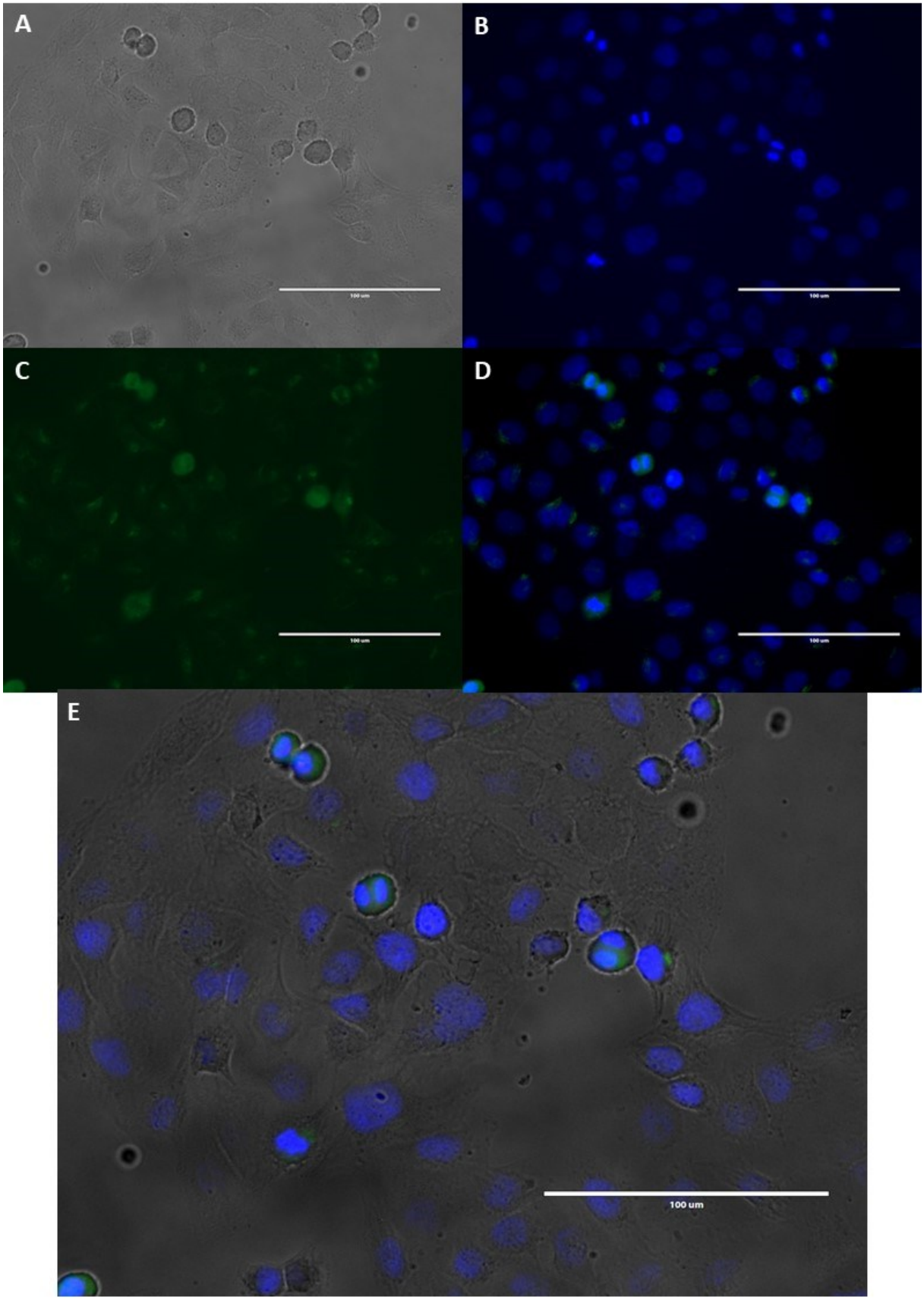

Figure 19: Optimization of GM130 visualisation, anti-GM130 1:2500 (magnification 40x); **A**) cells in bright-field, **B**) nuclei stained with DAPI (blue), **C**) visualised GM130 (green), **D**) visualised nuclei and GM130, **E**) images A-D merged.

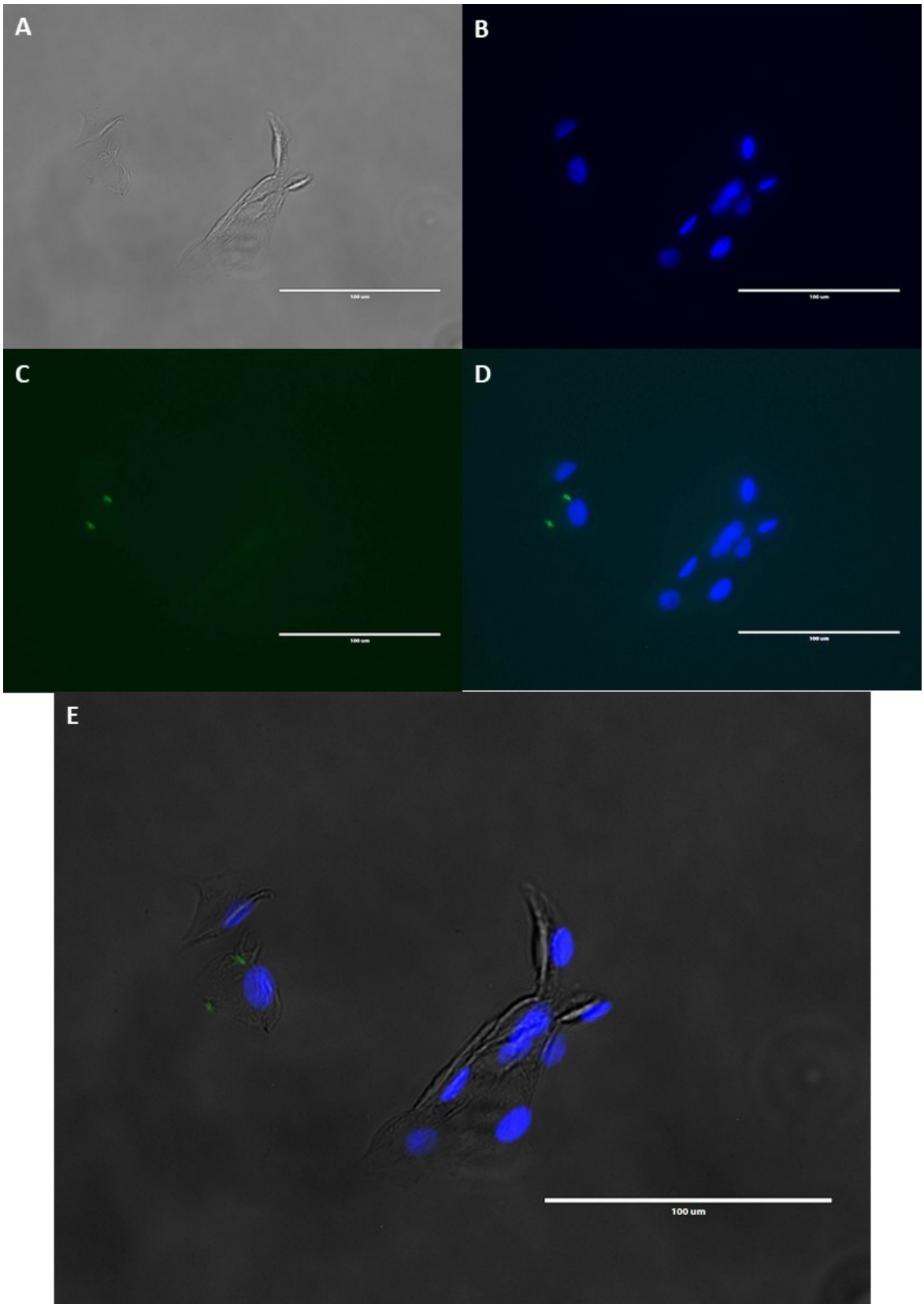

Figure 20: Verification of specificity binding of anti-rb IgG AF 488 (magnification 40x); **A**) cells in bright-field, **B**) nuclei stained with DAPI (blue), **C**) visualised anti-rb IgG AF 488 (green), **D**) visualised nuclei and anti-rb IgG AF 488, **E**) merged images A-D. AF – Alexa Fluor

6.3. Co-localization of FUBP3 and Golgi apparatus in HeLa cells

Using HeLa cells transfected with pCMV-FLAG-FUBP3 plasmid we were looking for a signal of GM130 protein and the signal of FUBP3. The signal of GM130 was observed in all cells of all experiments performed (Fig. 21 – 23), which indicates that the Golgi apparatus immunostaining was successful.

We detected a high signal of recombinant FUBP3-FLAG fragment using anti-FLAG antibody, that was specific for transfected cells. The FUBP3 was detected mainly in the cytosol of the cells, with a small portion of the protein located in the nucleus. From the image (Fig. 21 panel I), it seems that at least part of the protein pool is localized in the same region as the Golgi apparatus (Fig. 21). The same distribution of FUBP3 was observed in transfected cells using anti-FUBP3 antibodies (Fig. 22).

In the case of HeLa cells with native expression of FUBP3, the investigated protein was predominantly located around the nucleus of a small number of cells (Fig. 23). In the same cells, a certain degree of FUBP3 and Golgi apparatus co-localization can be seen (Fig. 23).

To make sure that there is no interference between secondary antibodies used to stain both GM130 and FUBP3 we performed a control experiment to detect any non-specific binding, i.e. immunostaining was performed without incubation with primary antibodies. No signal apart from the background was seen in either of images (Fig. 24)

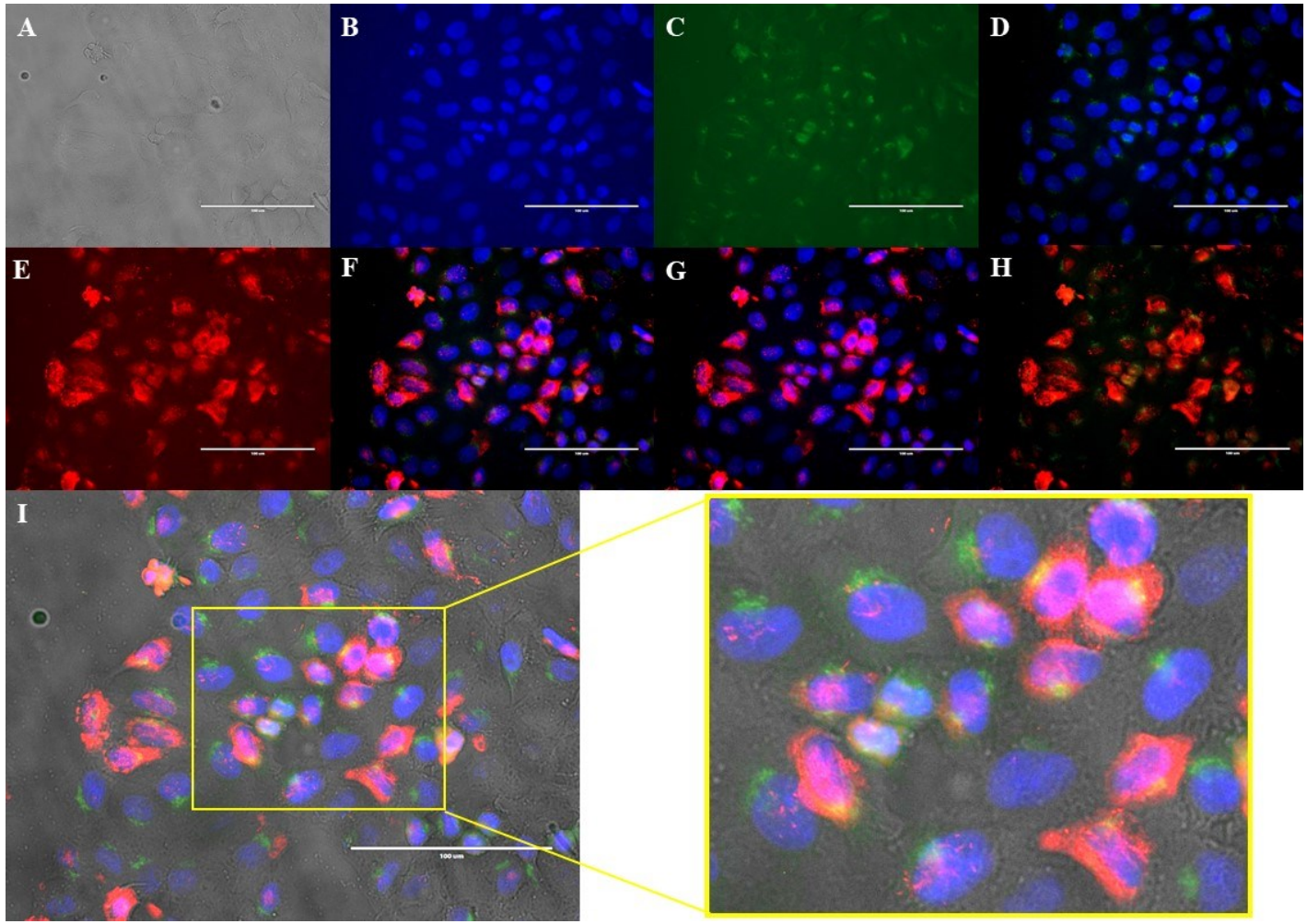

Figure 21: **Co-localization of FUBP3 and GM130, overexpressed FUBP3, anti-FLAG 1:1000** (magnification 40x); **A**) cells in bright field, **B**) visualised nuclei stained with DAPI (blue), **C**) visualised GM130 (green), **D**) visualised nuclei and GM130, **E**) visualised FUBP3 (red), **F**) visualised nuclei and FUBP3, **G**) visualised nuclei, GM130 and FUBP3, **H**) visualised GM130 and FUBP3, **I**) bright-field, visualised DAPI, GM130 and FUBP3.

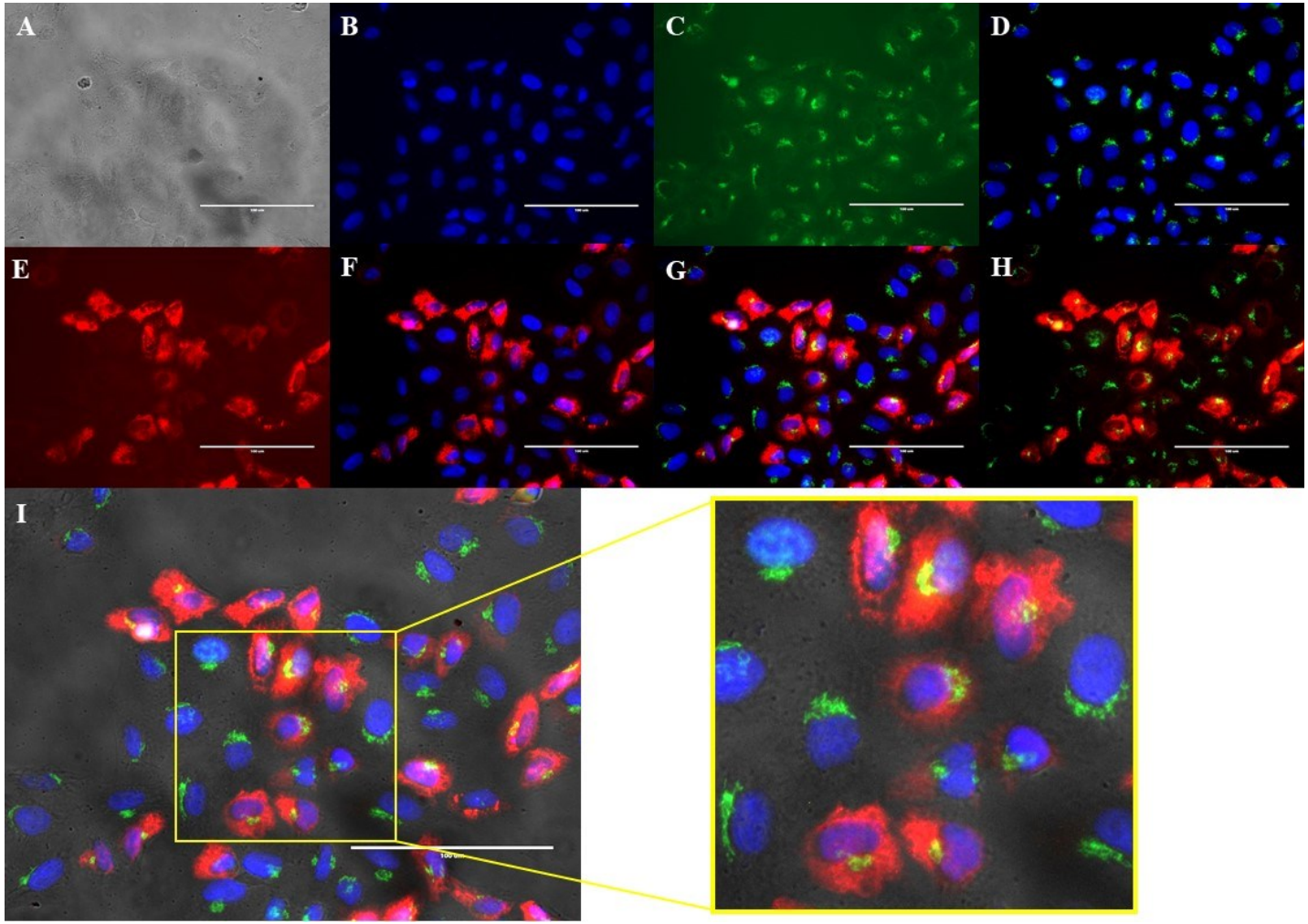

Figure 22: **Co-localization of FUBP3 and GM130, overexpressed FUBP3, anti-FUBP3 1:200** (magnification 40x); **A**) cells in bright field, **B**) visualised nuclei stained with DAPI (blue), **C**) visualised GM130 (green), **D**) visualised nuclei and GM130, **E**) visualised FUBP3 (red), **F**) visualised nuclei and FUBP3, **G**) visualised nuclei, GM130 and FUBP3, **H**) visualised GM130 and FUBP3, **I**) bright-field, visualised nuclei, GM130 and FUBP3.

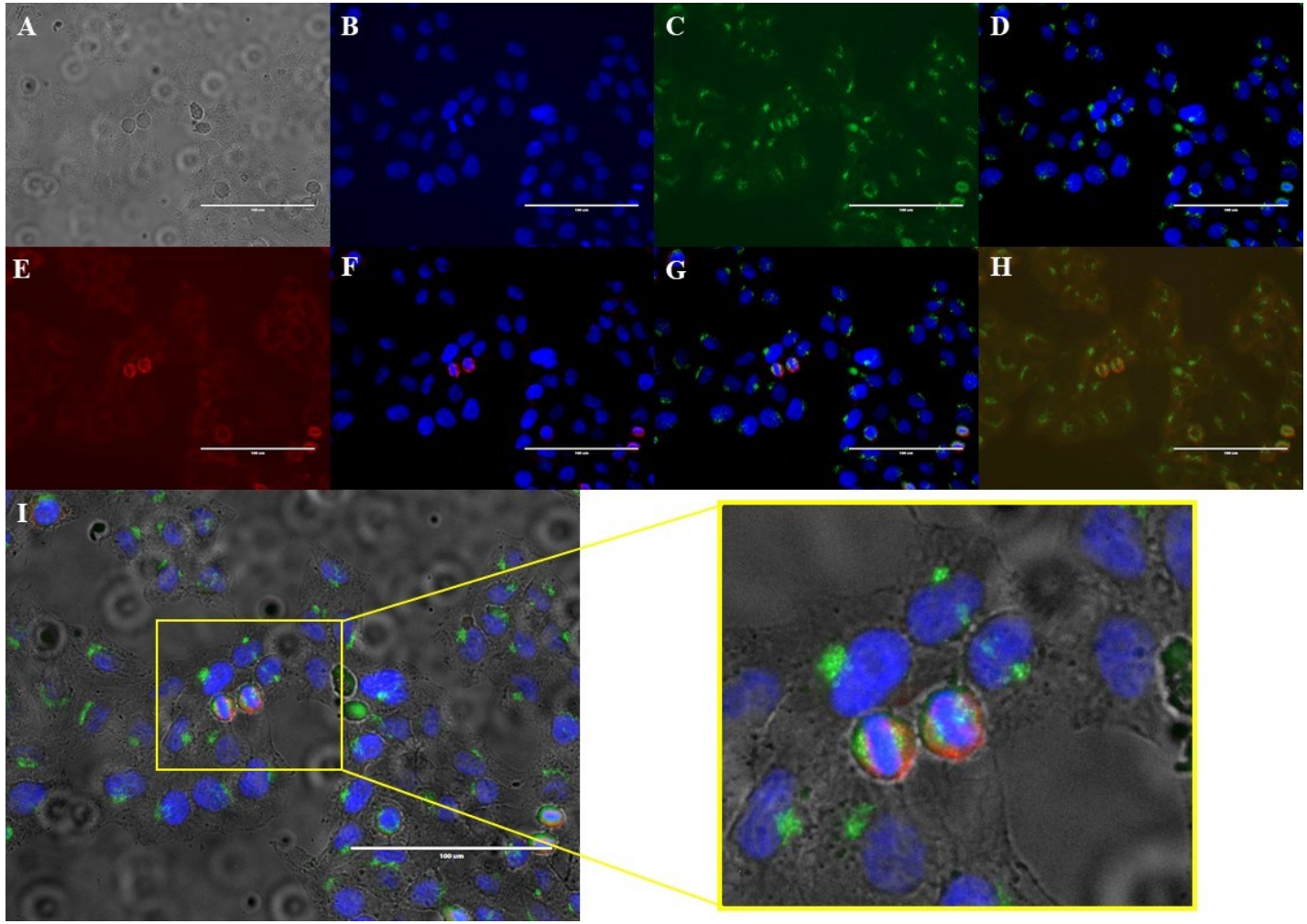

Figure 23: **Co-localization of FUBP3 and GM130, endogenous FUBP3, anti-FUBP3 1:200** (magnification 40x); **A**) cells in bright field, **B**) visualised nuclei stained with DAPI (blue), **C**) visualised GM130 (green), **D**) visualised nuclei and GM130, **E**) visualised FUBP3 (red), **F**) visualised nuclei and FUBP3, **G**) visualised nuclei, GM130 and FUBP3, **H**) visualised GM130 and FUBP3, **I**) bright-field, visualised nuclei, GM130 and FUBP3.

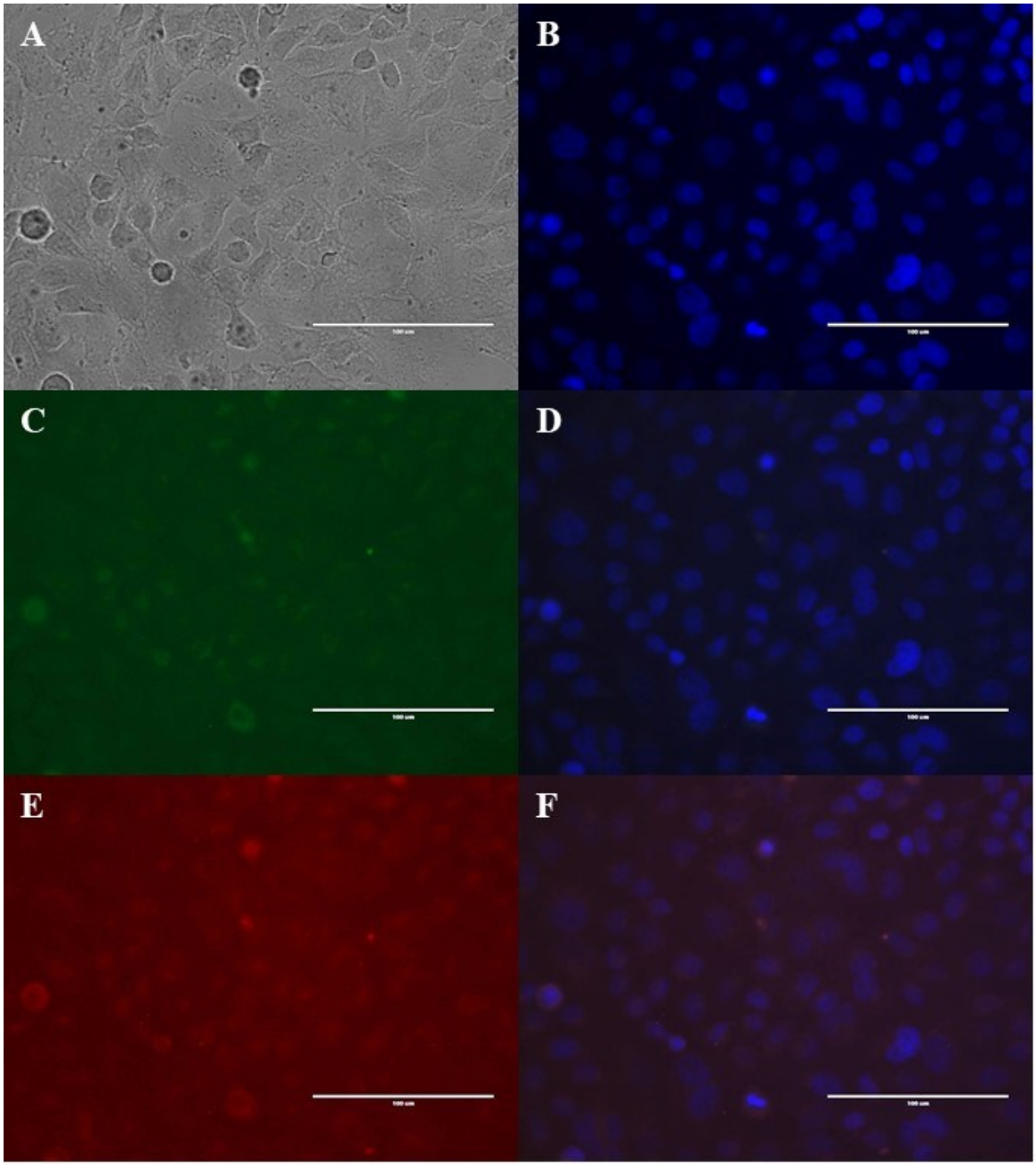

Figure 24: Verification of specificity of anti-ms IgG AF 555 and anti -rb IgG AF 488 (both 1:1000) (magnification 40x); **A**) cells in bright field, **B**) visualised nuclei stained with DAPI (blue), **C**) visualised anti-rb AF 488 (green) **D**) visualised nuclei and anti-rb AF 488 **E**) visualised anti-ms AF 555 (red) **F**) visualised nuclei and anti-ms AF 555. AF – Alexa Fluor

6.4. Silencing of FUBP3 expression

Gene silencing is a widely used technique in molecular biology for determining the function of the protein in a cell. That is the reason why we focused on establishing a protocol for silencing of *FUBP3* gene. The efficiency of gene silencing was determined using immunostaining for FUBP3 as described in 6.3., with the same concentrations of antibodies used.

In cells transfected with shRNA FUBP3, the expression of FUBP3 was diminished compared to cells with native production of FUBP3. This is especially visible in Figure 26 panel C where any FUBP3 signal would be visible. Only one cell showed strong bordered spots of the signal.

The possible off-target effects of chosen shRNA was evaluated using a rescue experiment; i.e., the pCMV-FLAG-FUBP3 plasmid was also introduced into FUBP3 shRNA silenced cells to abolish effects of the shRNA and restore the original phenotype. As seen in Fig 27, the signal was detected only in some cells. The FUBP3 signal is mostly located in sharply confined spaces around or within the nucleus.

Cells that have not been transfected with shRNA containing plasmid, but have been transfected with pCMV-FLAG-FUBP3 plasmid showed similar pattern and intensity of signal as in previously done experiments.

For negative control, a plasmid with scrambled shRNA was used and cells were stained with an anti-FUBP3 antibody. The localisation of FUBP3 changed in comparison with the localisation of endogenous FUBP3 protein. The protein FUBP3 was confined in small sharply bordered granules located around the cell nucleus.

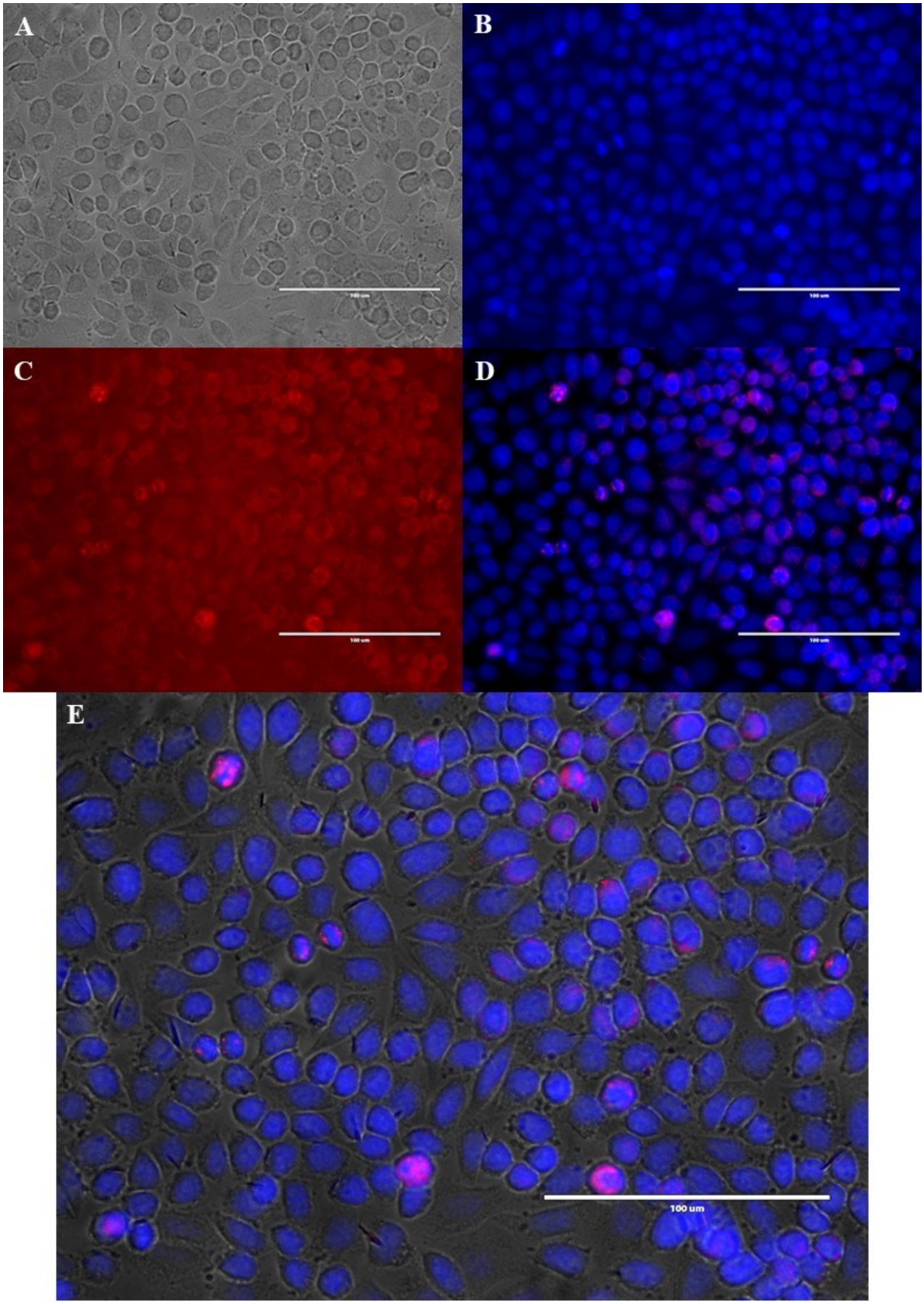

Figure 25: Silencing of FUBP3 expression, endogenous FUBP3, anti-FUBP3 (1:200) (magnification 40x); **A**) cells in bright-field, **B**) nuclei stained with DAPI (blue), **C**) visualisation of FUBP3 (red), **D**) nuclei and FUBP3, **E**) images A-D merged.

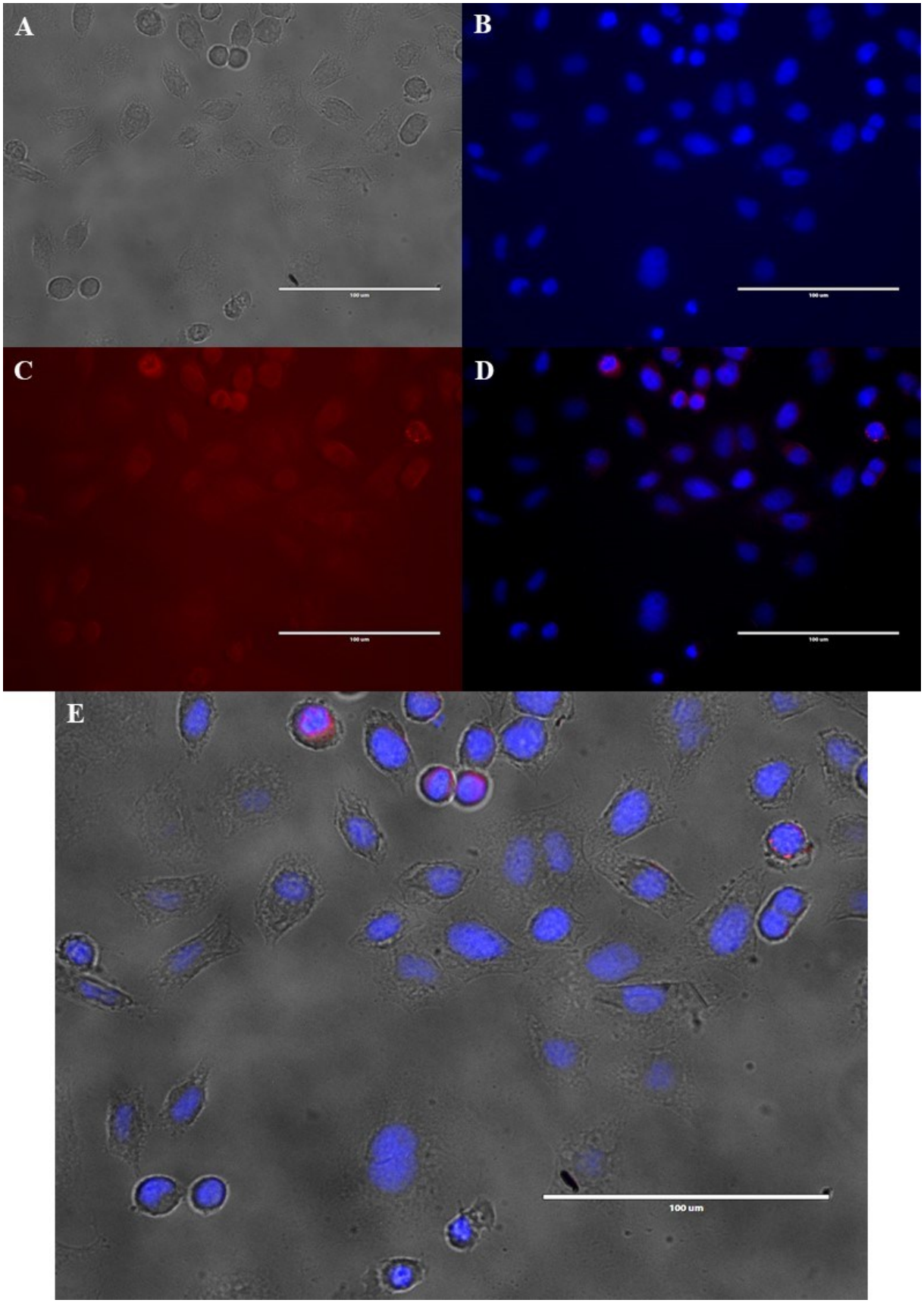

Figure 26: Silencing of FUBP3 expression, silenced FUBP3, anti-FUBP3 (1:200) (magnification 40x); **A**) cells in bright-field, **B**) nuclei stained with DAPI (blue), **C**) visualisation of FUBP3 (red), **D**) nuclei and FUBP3, **E**) images A-D merged.

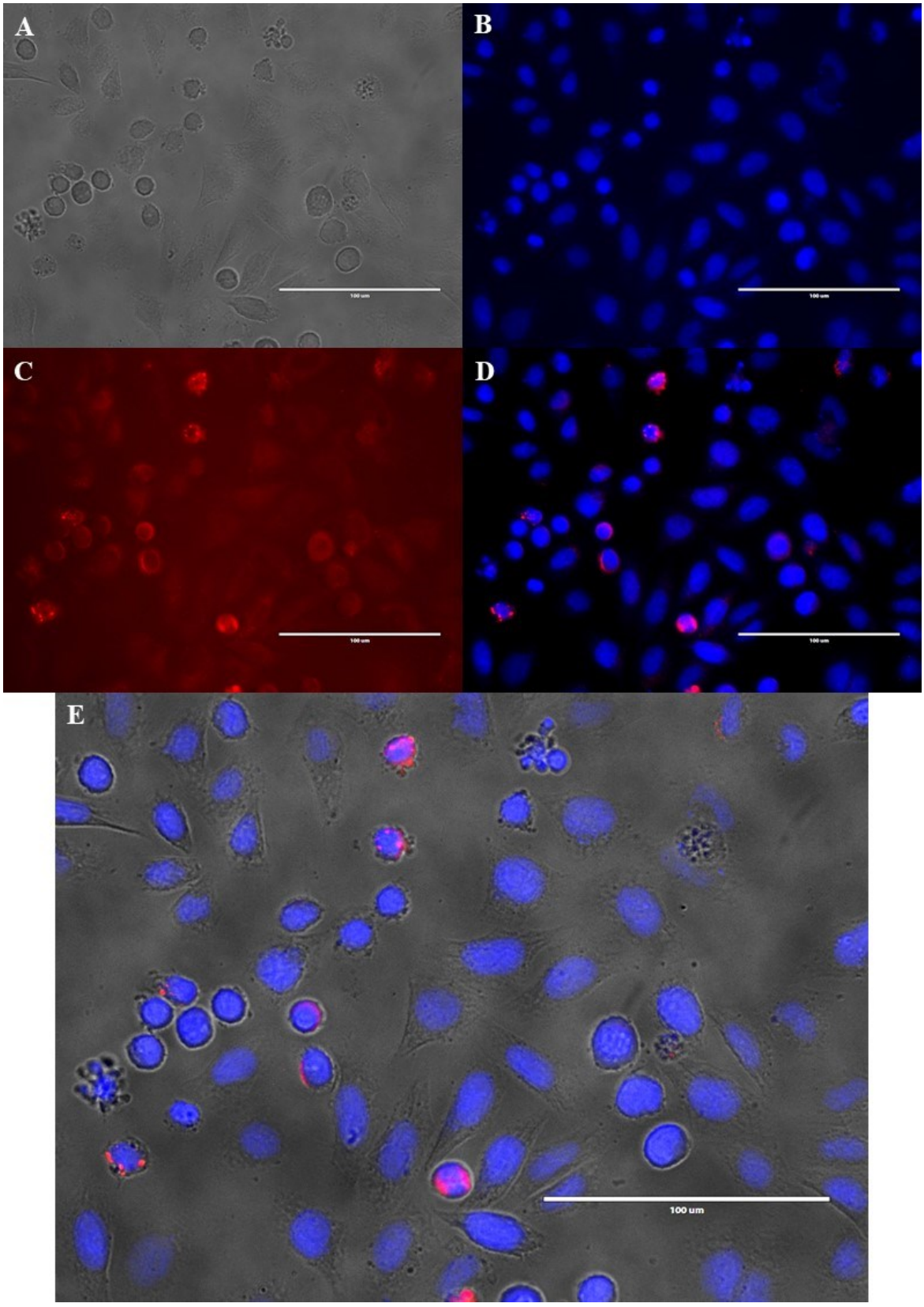

Figure 27: Silencing of FUBP3 expression, silenced FUBP3, transfected with pCMV-FLAG-FUBP3, anti-FUBP3 (1:200) (magnification 40x); **A**) cells in bright-field, **B**) nuclei stained with DAPI (blue), **C**) visualisation of FUBP3 (red), **D**) nuclei and FUBP3, **E**) images A-D merged

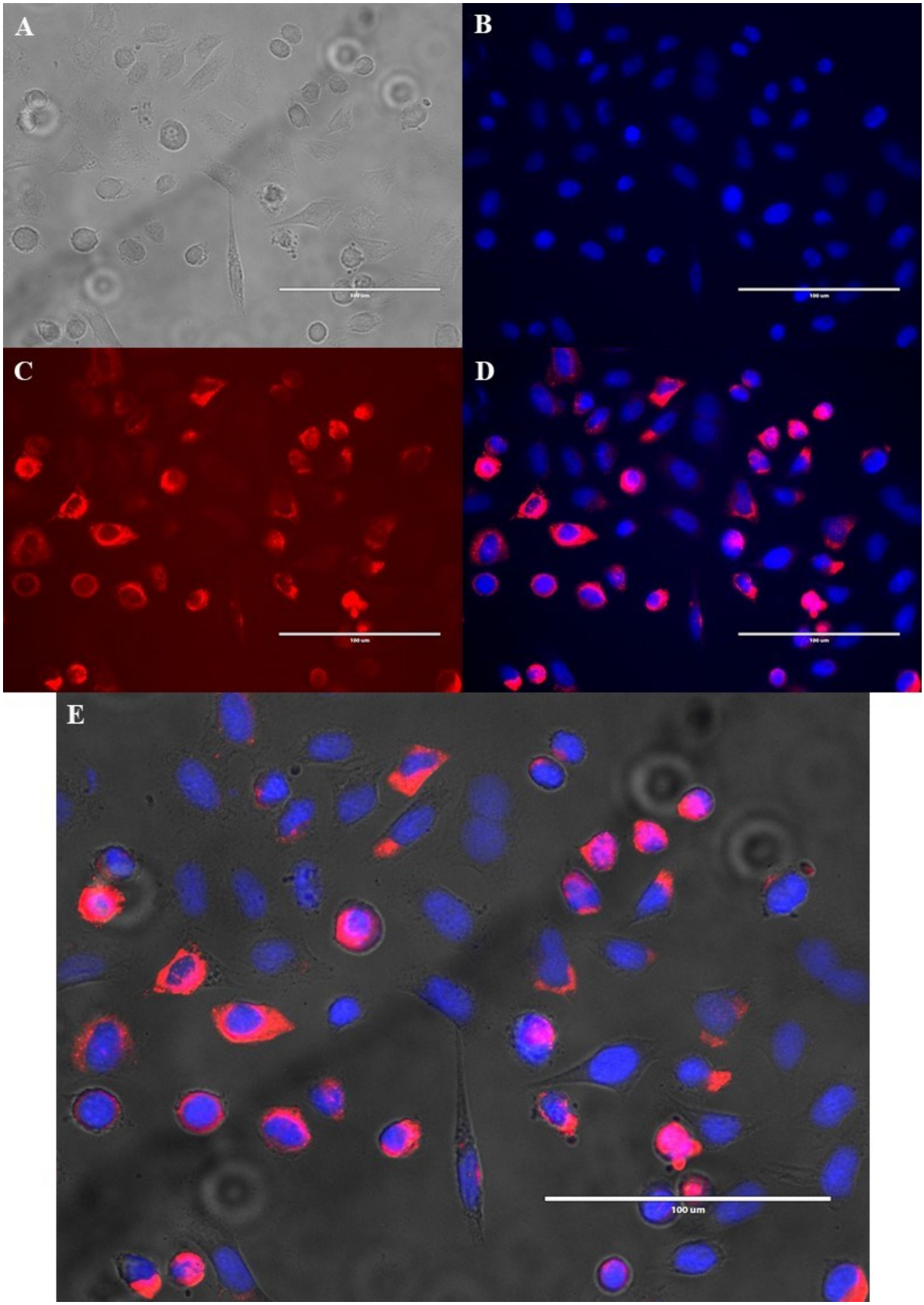

Figure 28: Silencing of FUBP3 expression, overexpressed FUBP3, anti-FUBP3 (1:200) (magnification 40x); **A**) cells in bright-field, **B**) nuclei stained with DAPI (blue), **C**) visualisation of FUBP3 (red), **D**) nuclei and FUBP3, **E**) images A-D merged.

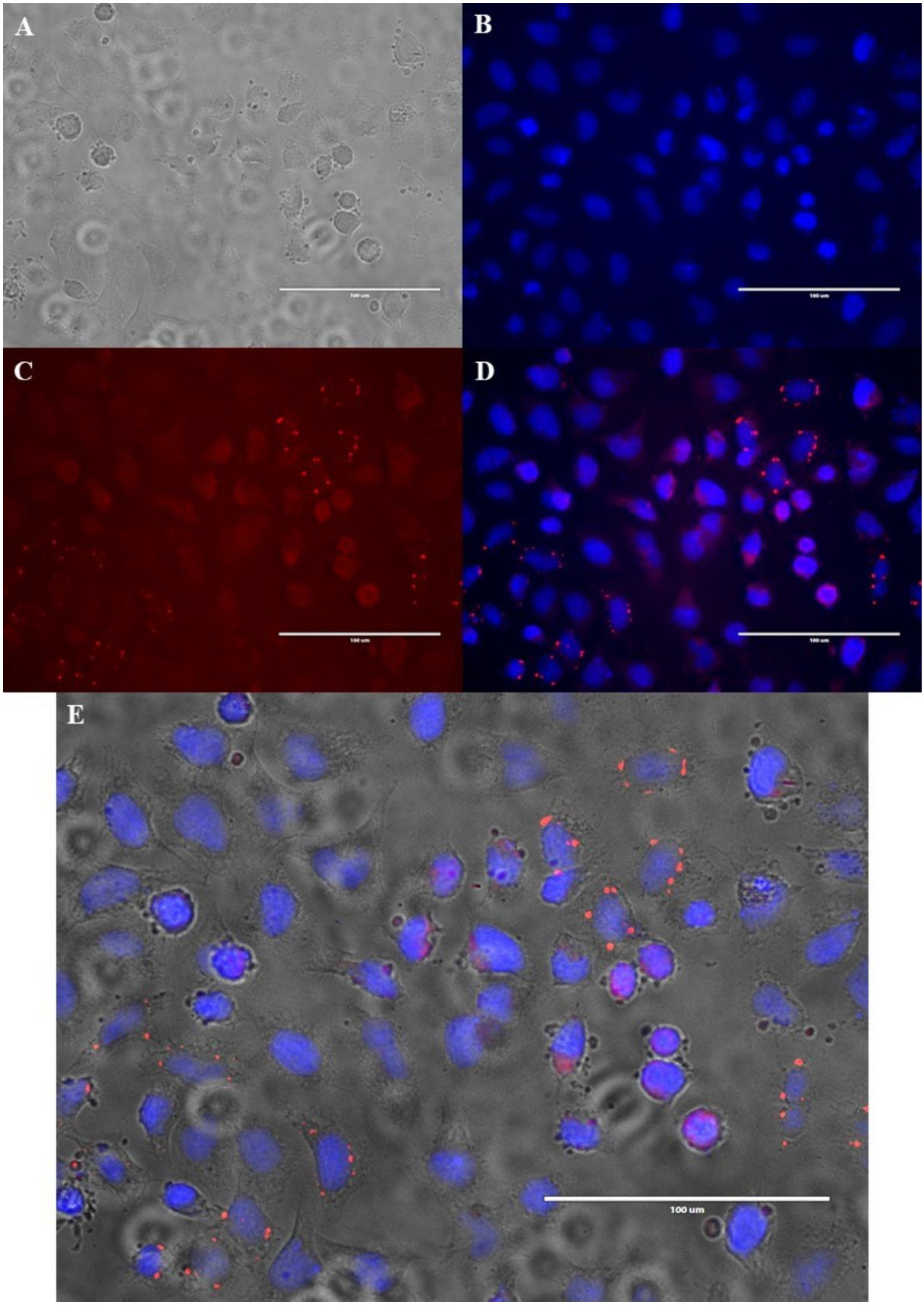

Figure 29: Silencing of FUBP3 expression, scrambled shRNA control, anti-FUBP3 (1:200) (magnification 40x); **A**) cells in bright-field, **B**) nuclei stained with DAPI (blue), **C**) visualisation of FUBP3 (red), **D**) nuclei and FUBP3, **E**) images A-D merged.

7. Discussion

Since the function of FUBP3 is not known and the localisation of the protein was poorly studied, this work aimed to analyse the localisation of FUBP3 in HeLa cells. Our hypothesis, that FUBP3 is predominantly localised in the cell nucleus was based on its proposed biological function. This hypothesis was also in line with the study done by He et al., 2000, which used HeLa cells to identify FUBP1 as a transcription factor localised in the cell nucleus. Having in mind, that this work is a pilot study for subsequent works investigating the function of FUBP3 and its role in osteoporosis, we have chosen immunostaining of the investigated protein and its subsequent visualisation with fluorescence microscopy.

We successfully localised FUBP3 in HeLa cells using immunofluorescence. On the contrary to the original hypothesis, the majority of the FUBP3 in the cells was localised throughout the entire cytoplasm with only a small fraction of the protein being located within the nucleus. There might be multiple reasons why this result was observed. First, the localisation might be dependent on the cell cycle phase. Since we have not used cells with synchronized cell cycle, we have been observing several cell populations with different localisation of FUBP3. Second, there are structural differences between each member of the FUBP family. FUBP3 does not share the same N-terminal bipartite nuclear localization signal (NLS) that as in both FUBP and FUBP2. NLS is an amino acid sequence that labels the proteins to be imported into the cell nucleus (He et al., 2000). In fact, FUBP3 only contains half of the NLS present in FUBP and FUBP2. It was reported that approximately 30 % to 60 % of the total cellular amount of FUBP3 is located in the nucleus. In contrast, FUBP and FUBP2 are almost completely nuclear (Chung et al., 2006).

The same study by Chung et al., 2006 also concluded that once FUBP3 is present in the cell nucleus, it is co-localized at the same nuclear sites as the remaining members of the FUBP family.

FUBP3's predominant localization in the cytoplasm might suggest that it also has some function there. As it was already mentioned in this work, the FUBP family contains the KH motif with RNA-binding properties. Several studies found out that FUBP3 binds to mRNA and regulates the translation of proteins such as immune activating ligand MICB and β-actin (Mukherjee et al., 2019; Nachmani et al., 2014). FUBP3 also binds to the

3’ untranslated region of thrombin mRNA in cooperation with FUBP2 in HUH7 hepatoma cells (Danckwardt et al., 2011). To determine whether mRNA binding of FUBP3 plays a role in the pathophysiology of osteoporosis further experiments are needed.

HeLa cells have a low natural expression of FUBP3, which could be seen in our experiments. Therefore, this cell line might not be an optimal cell line for investigation of the protein’s localisation. To confirm the results, we admit subsequent experiments using different cell lines are needed. To confirm the localisation of FUBP3 in the cell itself, a complementary method of tagging the FUBP3 for fluorescence microscopy such as recombinant protein is advisable.

The specificity of FUBP3 immunostaining was confirmed by the silencing experiment. The silencing itself was controlled by a rescue experiment and negative control using scrambled shRNA. Both control experiments were successful and thus proved that the silencing itself was successful and specific.

We successfully managed to use immunofluorescence co-localization of FUBP3 and GM130 to visualise both of the proteins in the cells. In case of using the co-localization of FUBP3 with Golgi apparatus to prove our hypothesis, the results we obtained in our experiments are inconclusive. Our preliminary results suggest that FUBP3 colocalized with Golgi apparatus marker GM130. The evaluation of co-localization is limited by the resolution of fluorescence microscope images. To improve the resolution of images, confocal laser high-resolution microscopy could yield better results.

We compared our images to images from RBP Image Database (Lecuyer Lab, 2020), a microscopy image database documenting the results of immunofluorescence experiment to characterise subcellular localization properties of human RNA binding proteins. Their results are consistent with the result from our experiments and there is no conclusive co localization of FUBP3 and Golgi apparatus in HeLa cells.

There are several limitations of this study, such as the chosen cell culture and evaluation of acquired images. As it was already stated, HeLa cells are not optimal for these experiments and for acquiring conclusive results that could be used to determine the role of FUBP3 in the pathophysiology of osteoporosis. The use of different cell lines originating from human bone tissue such as HOS would be more appropriate for further research in this field. Furthermore, cells’ characteristics change and their proliferation begin to decline with every passage, even in the immortalized cell lines. Consequently, a passage number might

have influenced the results and may contribute to a different level of protein expression. However, our experiments were performed using cells in close passage number.

The images were acquired usually in five sets originating from randomly selected regions of each coverslip. There is a possibility that the acquired images do not represent the true situation in the cell population, as the process of selection is subjective. Introducing an unbiased observer to choose the regions to acquire images might bring more objectivity to it. Furthermore, the introduction of a different and more independent method of image evaluation would increase the reliability of the results obtained.

8. Conclusion

In summary, FUBP3 protein is mainly localized in cell cytoplasm either in a small area around the nucleus membrane or diffused through the whole cytoplasm with a small fraction of the protein is in the nucleus. The co-localization experiment showed that FUBP3 is at least partially located in the Golgi apparatus.

We have partially confirmed starting hypothesis and the work can be perceived as successful. We have managed to visualise FUBP3 in HeLa cells using immunofluorescence. The specificity of the immunostaining was confirmed by silencing of FUBP3 expression, and the silencing experiment was proven to be successful and specific as a control. Therefore, the established protocol can be used as a starting point in experiments with other cell lines.

As for co-localization of FUBP3 with Golgi apparatus, we optimized the concentration of GM130 antibody to yield good results and successfully used immunostaining to visualise both structures at the same time. As with the protocol for localization of FUBP3 alone, this protocol can be subsequently used as a starting point for research in different cell lines.

This work was a pilot study focused for optimizing of immunofluorescent detection of target proteins. Further experiments using cell lines originating from bone tissues, such as HOS cell line, have been proposed as well as using complementary methods of visualisation of FUBP3 in cells.

9. References

1. Almeida M, Han L, Bellido T, Manolagas SC, Kousteni S. Wnt Proteins Prevent Apoptosis of Both Uncommitted Osteoblast Progenitors and Differentiated Osteoblasts by β-Catenin-dependent and -independent Signaling Cascades Involving Src/ERK and Phosphatidylinositol 3-Kinase/AKT. J Biol Chem 2005;280:41342–51. https://doi.org/10.1074/jbc.M502168200.
2. Athanasou NA, Quinn J. Immunophenotypic differences between osteoclasts and macrophage polykaryons: Immunohistological distinction and implications for osteoclast ontogeny and function. J Clin Pathol 1990:7.
3. Aubin JE. Bone Stem Cells. J Cell Biochem Suppls 1998;30:73–82.
4. Avigan MI, Strober B, Levens D. A Far Upstream Element Stimulates c-myc Expression in Undifferentiated Leukemia Cells. Journal of Biological Chemistry 1990;265:18538–45.
5. Bae S, Lee MJ, Mun SH, Giannopoulou EG, Yong-Gonzalez V, Cross JR, et al. MYC-dependent oxidative metabolism regulates osteoclastogenesis via nuclear receptor ERRα. Journal of Clinical Investigation 2017;127:2555–68. https://doi.org/10.1172/JCI89935.
6. Battaglino R, Kim D, Fu J, Vaage B, Fu X-Y, Stashenko P. c-myc Is Required for Osteoclast Differentiation. J Bone Miner Res 2002;17:763–73. https://doi.org/10.1359/jbmr.2002.17.5.763.
7. Behr B, Leucht P, Longaker MT, Quarto N. Fgf-9 is required for angiogenesis and osteogenesis in long bone repair. Proceedings of the National Academy of Sciences 2010;107:11853–8. https://doi.org/10.1073/pnas.1003317107.
8. Bonewald LF, Johnson ML. Osteocytes, mechanosensing and Wnt signaling. Bone 2008;42:606–15. https://doi.org/10.1016/j.bone.2007.12.224.
9. Bonnelye E, Chabadel A, Saltel F, Jurdic P. Dual effect of strontium ranelate: Stimulation of osteoblast differentiation and inhibition of osteoclast formation and resorption in vitro. Bone 2008;42:129–38. https://doi.org/10.1016/j.bone.2007.08.043.
10. Bouchireb N, Clark MS. Human Gene Mapping Report - Human FUSE binding 3 gene (FBP3). Chromosome Research 1999:557.
11. Bounjour P, Clark P, Cooper C, Dawson-Hughes B, De Laet C, Johansson H, et al. WHO Scientific Group on the Assesment of Osteoporosis at Primary Health Care Level 2004.

12. Boyce B, Yao Z, Xing L. Osteoclasts Have Multiple Roles in Bone in Addition to Bone Resorption. Crit Rev Eukar Gene Expr 2009;19:171–80. https://doi.org/10.1615/CritRevEukarGeneExpr.v19.i3.10.
13. Boyce BF, Xing L. Functions of RANKL/RANK/OPG in bone modeling and remodeling. Archives of Biochemistry and Biophysics 2008;473:139–46. https://doi.org/10.1016/j.abb.2008.03.018.
14. B110 Editor. Counting cells with a haemocytometer (Neubauer chamber). In: *Atlassian.* 2010. Available from: http://b110-wiki.dkfz.de/confluence/pages/viewpage.action?pageId=5931811. Accessed 15.2.2020
15. Chen JS, Sambrook PN. Antiresorptive therapies for osteoporosis: a clinical overview. Nat Rev Endocrinol 2012;8:81–91. https://doi.org/10.1038/nrendo.2011.146.
16. Chien H-L, Liao C-L, Lin Y-L. FUSE Binding Protein 1 Interacts with Untranslated Regions of Japanese Encephalitis Virus RNA and Negatively Regulates Viral Replication. Journal of Virology 2011;85:4698–706. https://doi.org/10.1128/JVI.01950-10.
17. Chung H-J, Liu J, Dundr M, Nie Z, Sanford S, Levens D. FBPs Are Calibrated Molecular Tools To Adjust Gene Expression. MCB 2006;26:6584–97. https://doi.org/10.1128/MCB.00754-06.
18. Cole ZA, Dennison EM, Cooper C. Osteoporosis epidemiology update. Curr Rheumatol Rep 2008;10:92–6. https://doi.org/10.1007/s11926-008-0017-6.
19. Danckwardt S, Gantzert A-S, Macher-Goeppinger S, Probst HC, Gentzel M, Wilm M, et al. p38 MAPK Controls Prothrombin Expression by Regulated RNA 3′ End Processing. Molecular Cell 2011;41:298 − 310. https://doi.org/10.1016/j.molcel.2010.12.032.
20. Datta HK, Ng WF, Walker JA, Tuck SP, Varanasi SS. The cell biology of bone metabolism. Journal of Clinical Pathology 2008;61:577–87. https://doi.org/10.1136/jcp.2007.048868.
21. Davis AC, Wims M, Spotts GD, Hann SR, Bradley A. A null c-myc mutation causes lethality before 10.5 days of gestation in homozygotes and reduced fertility in heterozygous female mice. Genes & Development 1993;7:671–82. https://doi.org/10.1101/gad.7.4.671.

22. Davis-Smyth T, Duncan RC, Zheng T, Michelotti G, Levens D. The Far Upstream Element-binding Proteins Comprise an Ancient Family of Single-strand DNA-binding Transactivators. J Biol Chem 1996;271:31679–87. https://doi.org/10.1074/jbc.271.49.31679.

23. DePinho RA, Schreiber-Agus N, Alt FW. myc Family Oncogenes in the Development of Normal and Neoplastic Cells. Advances in Cancer Research, vol. 57, Elsevier; 1991, p. 1–46. https://doi.org/10.1016/S0065-230X(08)60994-X.

24. Dimitriou R, Tsiridis E, Giannoudis PV. Current concepts of molecular aspects of bone healing. Injury 2005;36:1392–404. https://doi.org/10.1016/j.injury.2005.07.019.

25. Duncan R, Bazar L, Michelotti G, Tomonaga T, Krutzsch H, Avigan M, et al. A sequence-specific, single-strand binding protein activates the far upstream element of c-myc and defines a new DNA-binding motif. Genes & Development 1994;8:465–80. https://doi.org/10.1101/gad.8.4.465.

26. Estrada K, Styrkarsdottir U, Evangelou E, Hsu Y-H, Duncan EL, Ntzani EE, et al. Genome-wide meta-analysis identifies 56 bone mineral density loci and reveals 14 loci associated with risk of fracture. Nat Genet 2012;44:491–501. https://doi.org/10.1038/ng.2249.

27. Franz-Odendaal TA, Hall BK, Witten PE. Buried alive: How osteoblasts become osteocytes. Dev Dyn 2006;235:176–90. https://doi.org/10.1002/dvdy.20603.

28. Gau B-H, Chen T-M, Shih Y-HJ, Sun HS. FUBP3 interacts with FGF9 3′ microsatellite and positively regulates FGF9 translation. Nucleic Acids Research 2011;39:3582–93. https://doi.org/10.1093/nar/gkq1295.

29. Gearhart J, Pashos EE, Prasad MK. Pluripotency Redux — Advances in Stem-Cell Research. N Engl J Med 2007;357:1469–72. https://doi.org/10.1056/NEJMp078126.

30. Glass DA, Bialek P, Ahn JD, Starbuck M, Patel MS, Clevers H, et al. Canonical Wnt Signaling in Differentiated Osteoblasts Controls Osteoclast Differentiation. Developmental Cell 2005;8:751–64. https://doi.org/10.1016/j.devcel.2005.02.017.

31. He L, Weber A, Levens D. Nuclear targeting determinants of the far upstream element binding protein, a c-myc transcription factor. Nucleic Acids Research 2000;28:4558–65. https://doi.org/10.1093/nar/28.22.4558.

32. Heino T, Hentunen T. Differentiation of Osteoblasts and Osteocytes from Mesenchymal Stem Cells. CSCR 2008;3:131–45. https://doi.org/10.2174/157488808784223032.

33. Holick MF. Vitamin D Deficiency. New England Journal of Medicine 2007:16.
34. Johnson ML, Harnish K, Nusse R, Van Hul W. LRP5 and Wnt Signaling: A Union Made for Bone. J Bone Miner Res 2004;19:1749–57. https://doi.org/10.1359/JBMR.040816.
35. Kanis JA, Johnell O, Oden A, Johansson H, McCloskey E. FRAXTM and the assessment of fracture probability in men and women from the UK. Osteoporos Int 2008;19:385–97. https://doi.org/10.1007/s00198-007-0543-5.
36. Kanis JA, Rizzoli R, Reginster J-Y. European guidance for the diagnosis and management of osteoporosis in postmenopausal women. Osteoporos Int 2019;30:3–44. https://doi.org/10.1007/s00198-018-4704-5.
37. Kikuchi A, Yamamoto H, Sato A. Selective activation mechanisms of Wnt signaling pathways. Trends in Cell Biology 2009;19:119–29. https://doi.org/10.1016/j.tcb.2009.01.003.
38. Kobayashi Y, Uehara S, Udagawa N. Roles of non-canonical Wnt signaling pathways in bone resorption. Journal of Oral Biosciences 2018;60:31–5. https://doi.org/10.1016/j.job.2018.03.001.
39. Kratchmarova I, Blagoev B, Haack-Sorensen M, Kassem M, Mann M. Mechanism of Divergent Growth Factor Effects in Mesenchymal Stem Cell Differentiation. Science 2005;308:1472–7. https://doi.org/10.1126/science.1107627.
40. Lecuyer Lab. RBP Image Database. In: *RBP Image Database.* 2020. Available from: http://rnabiology.ircm.qc.ca/RBPImage/marker.php?cell=Hela&targets=FUBP3&markers=GM130. Accessed 1.3.2020
41. Liu J, Kouzine F, Nie Z, Chung H-J, Elisha-Feil Z, Weber A, et al. The FUSE/FBP/FIR/TFIIH system is a molecular machine programming a pulse of c-myc expression. EMBO J 2006;25:2119–30. https://doi.org/10.1038/sj.emboj.7601101.
42. Malbon C C. Frizzleds: new members of the superfamily of G-protein-coupled receptors. Front Biosci 2004;9:1048. https://doi.org/10.2741/1308.
43. Marie PJ, Felsenberg D, Brandi ML. How strontium ranelate, via opposite effects on bone resorption and formation, prevents osteoporosis. Osteoporos Int 2011;22:1659–67. https://doi.org/10.1007/s00198-010-1369-0.
44. Mateyak MK, Obaya AJ, Adachi S, Sedivy JM. Phenotypes of c-Myc-deficient Rat Fibroblasts Isolated by Targeted Homologous Recombination. Cell Growth & Differentiation 1997;8:1039–48.

45. McMahon SB. MYC and the Control of Apoptosis. Cold Spring Harbor Perspectives in Medicine 2014;4:a014407–a014407. https://doi.org/10.1101/cshperspect.a014407.
46. Miller SC, Bowman BM, Smith JM, Jee WSS. Characterization of endosteal bone-lining cells from fatty marrow bone sites in adult beagles. Anat Rec 1980;198:163–73. https://doi.org/10.1002/ar.1091980204.
47. Mosekilde L, Torring O, Rejnmark L. Emerging Anabolic Treatments in Osteoporosis. CDS 2011;6:62–74. https://doi.org/10.2174/157488611795684712.
48. Mukherjee J, Hermesh O, Eliscovich C, Nalpas N, Franz-Wachtel M, Maček B, et al. β-Actin mRNA interactome mapping by proximity biotinylation. Proc Natl Acad Sci USA 2019;116:12863–72. https://doi.org/10.1073/pnas.1820737116.
49. Nachmani D, Gutschner T, Reches A, Diederichs S, Mandelboim O. RNA-binding proteins regulate the expression of the immune activating ligand MICB. Nat Commun 2014;5:4186. https://doi.org/10.1038/ncomms5186.
50. Nakamura I, Duong LT, Rodan SB, Rodan GA. Involvement of αvβ3 integrins in osteoclast function. J Bone Miner Metab 2007;25:337–44. https://doi.org/10.1007/s00774-007-0773-9.
51. National Institute for Health and Care Excelence. Osteoporosis: assessing the risk of fragility fracture 2017.
52. NIH Consensus Development Panel on Osteoporosis Prevention, Diagnosis, and Therapy. Osteoporosis Prevention, Diagnosis, and Therapy. JAMA: The Journal of the American Medical Association 2001;285:785–95. https://doi.org/10.1001/jama.285.6.785.
53. O'Brien CA, Nakashima T, Takayanagi H. Osteocyte control of osteoclastogenesis. Bone 2013;54:258–63. https://doi.org/10.1016/j.bone.2012.08.121.
54. Olanich ME, Moss BL, Piwnica-Worms D, Townsend RR, Weber JD. Identification of FUSE-binding protein 1 as a regulatory mRNA-binding protein that represses nucleophosmin translation. Oncogene 2011;30:77–86. https://doi.org/10.1038/onc.2010.404.
55. Palumbo C, Palazzini S, Zaffe D, Marotti G. Osteocyte Differentiation in the Tibia of Newborn Rabbit: An Ultrastructural Study of the Formation of Cytoplasmic Processes. Acta Anatomica 1990;137:350–8. https://doi.org/10.1159/000146907.

56. Parfitt AM. Osteonal and hemi-osteonal remodeling: The spatial and temporal framework for signal traffic in adult human bone. J Cell Biochem 1994;55:273–86. https://doi.org/10.1002/jcb.240550303.

57. Park SR, Oreffo ROC, Triffitt JT. Interconversion potential of cloned human marrow adipocytes in vitro. Bone 1999;24:549–54. https://doi.org/10.1016/S8756-3282(99)00084-8.

58. Reginster J-Y, Burlet N. Osteoporosis: A still increasing prevalence. Bone 2006;38:4–9. https://doi.org/10.1016/j.bone.2005.11.024.

59. Rocha-Braz MGM, Ferraz-de-Souza B. Genetics of osteoporosis: searching for candidate genes for bone fragility. Arch Endocrinol Metab 2016;60:391–401. https://doi.org/10.1590/2359-3997000000178.

60. Rossini M, Gatti D, Adami S. Involvement of WNT/b-catenin Signaling in the Treatment of Osteoporosis. Calcif Tissue Int 2013;93:121–32. https://doi.org/DOI 10.1007/s00223-013-9749-z.

61. Schaffler MB, Cheung W-Y, Majeska R, Kennedy O. Osteocytes: Master Orchestrators of Bone. Calcif Tissue Int 2014;94:5–24. https://doi.org/10.1007/s00223-013-9790-y.

62. SignaGen Laboratories. PolyJet™ In Vitro DNA Transfection Reagent. In: *SignaGen Laboratories*. 2020. Available from: https://signagen.com/In-Vitro-DNA-Transfection-Reagents/SL100688/PolyJet-DNA-In-Vitro-Transfection-Reagent. Accessed 5.3.2020

63. Siomi H, Matunis MJ, Michael WM, Dreyfuss G. The pre-mRNA binding K protein contains a novel evolutionarily conserved motif. Nucleic Acids Research 1993;21:1193–8.

64. Soysa NS, Alles N, Aoki K, Ohya K. Osteoclast formation and differentiation: An overview. J Med Dent Sci 2012:65–74.

65. Svedbom A, Hernlund E, Ivergård M, Compston J, Cooper C, Stenmark J, et al. Osteoporosis in the European Union: a compendium of country-specific reports. Arch Osteoporos 2013;8:137. https://doi.org/10.1007/s11657-013-0137-0.

66. Teitelbaum SL. Bone Resorption by Osteoclasts. Science 2000;289:1504–8. https://doi.org/10.1126/science.289.5484.1504.

67. Tian E, Zhan F, Walker R, Rasmussen E, Ma Y, Barlogie B, et al. The Role of the Wnt-Signaling Antagonist DKK1 in the Development of Osteolytic Lesions in

Multiple Myeloma. N Engl J Med 2003;349:2483–94. https://doi.org/10.1056/NEJMoa030847.

68. Trajanoska K, Morris JA, Oei L, Zheng H-F, Evans DM, Kiel DP, et al. Assessment of the genetic and clinical determinants of fracture risk: genome wide association and mendelian randomisation study. BMJ 2018:k3225. https://doi.org/10.1136/bmj.k3225.
69. Vestergaard P, Rejnmark L, Mosekilde L. Osteoporosis is markedly underdiagnosed: a nationwide study from Denmark. Osteoporos Int 2005;16:134–41. https://doi.org/10.1007/s00198-004-1680-8.
70. Vindigni A, Ochem A, Gianluca T, Falaschi A. Identification of human DNA helicase V with the far upstream element-binding protein. Nucleic Acids Research 2001;29:1061–7. https://doi.org/10.1093/nar/29.5.1061.
71. Visscher PM, Brown MA, McCarthy MI, Yang J. Five Years of GWAS Discovery. The American Journal of Human Genetics 2012;90:7–24. https://doi.org/10.1016/j.ajhg.2011.11.029.
72. Wada T, Nakashima T, Hiroshi N, Penninger JM. RANKL–RANK signaling in osteoclastogenesis and bone disease. Trends in Molecular Medicine 2006;12:17–25. https://doi.org/10.1016/j.molmed.2005.11.007.
73. Walsh MC, Choi Y. Biology of the RANKL–RANK–OPG System in Immunity, Bone, and Beyond. Front Immunol 2014;5. https://doi.org/10.3389/fimmu.2014.00511.
74. Weber A, Kristiansen I, Johannsen M, Oelrich B, Scholmann K, Gunia S, et al. The FUSE binding proteins FBP1 and FBP3 are potential c-myc regulators in renal, but not in prostate and bladder cancer. BMC Cancer 2008;8:369. https://doi.org/10.1186/1471-2407-8-369.
75. Weinbaum S, Cowin SC, Zeng Y. A model for the excitation of osteocytes by mechanical loading-induced bone fluid shear stresses. Journal of Biomechanics 1994;27:339–60. https://doi.org/10.1016/0021-9290(94)90010-8.
76. Zhang J, Chen QM. Far upstream element binding protein 1: a commander of transcription, translation and beyond. Oncogene 2013;32:2907–16. https://doi.org/10.1038/onc.2012.350.
77. Zheng Y, Miskimins WK. Far upstream element binding protein 1 activates translation of p27Kip1 mRNA through its internal ribosomal entry site. The International Journal of Biochemistry & Cell Biology 2011;43:1641–8. https://doi.org/10.1016/j.biocel.2011.08.001.